Mathematical and Computational Applications

MDPI

Article

A Mathematical Study of Effects of Alzheimer's Drug Donepezil Hydrochloride on Neuronal Viscoelasticity and Action Potentials

Corina S. Drapaca

Department of Engineering Science and Mechanics, Pennsylvania State University, University Park, PA 16802, USA; csd12@psu.edu

Abstract: Alzheimer's disease (AD) is a degenerative disorder characterized by progressive cognitive decline and memory loss. The few contemporary therapies may ease symptoms and/or slow down AD progression but cannot cure the disease. The orally administered AD drug donepezil hydrochloride enhances the availability of acetylcholine that supports cholinergic neurotransmission. In this paper, a generalized Hodgkin-Huxley model is proposed that uses Caputo fractional order temporal derivatives to link action potentials and viscoelasticity of cholinergic receptors. The model provides not only structurally dependent action potentials for health and AD but also a possible mechanism of donepezil effect on action potentials: the binding between the acetylcholine and the receptors preserves the structural fitness of these receptors. In addition, a generalized pharmacokinetic model of donepezil transport to the brain is proposed that incorporates controlled release modalities. Caputo fractional order temporal derivatives are used again to model anomalous drug release. Numerical simulations show how controlled release donepezil recovers the structural integrity of the receptors which further brings the abnormal action potentials due to AD to their healthy state. The results suggest that combining various drug release modalities and dosages may improve treatment effectiveness with donepezil.

Keywords: fractional calculus; viscoelasticity; action potentials; Alzheimer's disease; donepezil

Citation: Drapaca, C.S. A Mathematical Study of Effects of Alzheimer's Drug Donepezil Hydrochloride on Neuronal Viscoelasticity and Action Potentials. *Math. Comput. Appl.* **2024**, *29*, 117. https://doi.org/10.3390/mca29060117

Academic Editor: Sundeep Singh

Received: 27 October 2024
Revised: 9 December 2024
Accepted: 10 December 2024
Published: 12 December 2024

1. Introduction

The first case of Alzheimer's disease (AD) was diagnosed in 1906 [1]. More than a century later, there are tens of millions of people with AD worldwide and millions of new cases are confirmed annually [2]. Currently, AD is considered to be a multifactorial degenerative disorder of the neuro-glial-vascular units characterized by progressive cognitive and memory deficits. The few existing therapies may ease symptoms and/or slow down AD progression but cannot cure the disease.

The lack of a cure and effective treatments for AD is because of the complexities of brain's structure and biochemical processes that have hindered the discovery of critical mechanisms governing the AD onset and progression. Pathological factors like the aggregation of toxic extracellular amyloid-β ($A\beta$) plaques, the accumulation of intracellular tau-containing neurofibrillary tangles (NFT) and the rise in neuroinflammation [3], as well as the intricate interlinks among them are presently considered possible causes of AD. For instance, the large loss of cells in the amygdala, hippocampus, and neocortex disrupts the cholinergic neurotransmission that leads to cognitive and functional dysfunctions. The accumulation of NFT causes the loss of neuronal functionality and eventually neuronal apoptosis. The aggregation of toxic $A\beta$ plaques impedes the clearance of brain waste via the glymphatic pathway and the blood-brain barrier which leads to neuroinflammation and neurodegeneration [4,5]. Cerebral chronic inflammation due to prolonged activation of microglia cells and astrocytes contributes not only to neurodegeneration but also to the aggregation of $A\beta$ plaques and NFT [6].

Given the rather futile attempts at treating AD by tackling various aspects of the accumulations of $A\beta$ plaques and NFT [7], recent years have seen renewed efforts in understanding the interplay between neurodegeneration, characterized by abnormal action potentials and damaged neuronal structure, and the buildups of $A\beta$ plaques and NFT that can improve the AD therapies aimed at enhancing the cholinergic neurotransmission [8–17]. One of the few FDA-approved drugs for treating AD that is safe and provides cognitive benefits at all stages of the disease is donepezil hydrochloride [7,18]. Donepezil is a fast-acting and reversible inhibitor of acetylcholinesterase (AChE), an enzyme that becomes abundant during AD progression and may be involved in the formation of the $A\beta$ plaques [7,8]. Specifically, the presence of $A\beta$ plaques increases the amount of one molecular form of AchE, while the accumulation of NFT causes an increase in the levels of all major molecular forms of AChE [8]. AChE disintegrates acetylcholine (ACh), a key neurotransmitter released by neurons involved in neuronal communications through binding to cholinergic ACh receptors [19,20]. Nicotinic and muscarinic receptors are the two main types of cholinergic ACh receptors. Nicotinic receptors are ligand-gated ion channels whose structural conformations are temporarily changed by the ACh binding to allow the fast depolarization of the postsynaptic neuronal membrane. Muscarinic receptors are G-protein coupled receptors that, when binded to ACh, activate intracellular signaling pathways via the G-proteins that cause the opening/closing of neuronal ion channels (hyperpolarization/depolarization of the membrane) and other slower cellular responses. The binding between AChE and donepezil increases temporarily the bioavailability of ACh and, thus, improves cholinergic transmission. Additionally, donepezil and its analogues are involved in the enhancement of cerebral blood flow and the reduction of neuroinflammation and oxidative stress and thus they may inhibit the aggregation of the $A\beta$ plaques [7,21].

Donepezil lessens AD symptoms but, as the disease progresses and negatively impacts the individual functions of the two types of cholinergic ACh receptors and the functional crosstalks between them [22,23], its dosage is increased gradually which can worsen gastrointestinal and heart-related adverse effects of the drug. To reduce side effects, various delivery and release systems for donepezil were proposed in the literature. For example, some donepezil-loaded systems that can reach the brain and provide nontoxic prolonged drug release are mango gum polymeric nanoparticles [24], extracellular vesicles isolated from human plasma [25], solid lipid nanoparticles with or without ApoE [26,27], cholesterol-modified pullulan nanoparticle with polysorbate 80 surface coverage [28], ternary sodium alginate based hydrogels [29], lyotropic liquid crystalline mesophases composed by monoolein/oleic acid/water [30], and sodium alginate microspheres [31]. Although in clinical practice donepezil is administered orally, nasal [32–34], subcutaneous [35] and transdermal [36] administrations have also been investigated and shown promising results.

Two aspects relevant to improving the treatment with donepezil that need more clarification are: (1) finding controlled release modalities for donepezil that provide effective treatments for longer time periods without increasing the drug dosage, and (2) finding mechanisms that link donepezil intake and action potentials. Mathematical modeling can provide insights into brain's processes and mechanisms worthy of further experimental/clinical explorations which ultimately may lead to better therapies for AD. Mathematical models of drug release (Fick, Higuchi, Hopfenberg Peppas, Weibull, etc. models) existing in the pharmacology literature predict cumulative drug release over time and can be easily fitted to experimental data [37,38]. In particular, the Ritger-Peppas model was used in experimental studies of controlled release donepezil to describe both Fickian and non-Fickian temporal release behavior [31]. The transport of a drug through the body can be described mathematically using pharmacokinetic (compartmental) models [39–41]. Specifically, pharmacokinetic models fitted to experimental observations of the transport of orally and nasally administrated donepezil were given in [32]. Lastly, the propagation of action potentials can be described mathematically by the Hodgkin-Huxley model [42] (see also [43]). Mathematical models of action potentials in the presence of AD were proposed in [44–46]. These models are obtained by coupling the Hodgkin-Huxley model and ion

concentration dynamics specific to AD via the Nernst equations. Potential linkages among the above-mentioned pharmacokinetic and Hodgkin-Huxley mathematical models have not been explored yet.

In this paper, a mathematical model that couples controlled release of donepezil, transport to the brain of donepezil, and the effect of donepezil on action potentials is proposed to study the two aspects stated earlier. The model's main assumptions are that: (1) AD onset and progression cause structural damages to the ion channels within a neuronal membrane that lead to abnormal action potentials, and (2) in the presence of AD and donepezil intake, the binding between ACh and ligand-gated ion channels temporarily recovers the structural fitness of the channels accompanied by healthy action potentials. These assumptions are supported by [10–12] (assumption 1) and respectively [47,48] (assumption 2). Mathematically, the coupling is realized through fractional order derivatives, versatile integro-differential operators that have been successfully used to model long-range (spatial) interactions and long-term (temporal) memory characteristic to various systems. Specifically, anomalous diffusion (diffusion process characterized by a non-linear power law relationship between the mean squared displacement of a particle and time) [49] and viscoelastic fading memory (distant past deformations have less influence on the present state than those which happened in the more recent past) [50] have been modeled with fractional order derivatives and these modeling techniques are also used in this paper. Thus, a generalized pharmacokinetic model for the transport of donepezil with anomalous release patterns is proposed that combines the pharmacokinetic model in [32] and the controlled release modalities in [31]. Also, a generalized Hodgkin-Huxley model linking the electric activity of neuronal membrane (action potentials) and the viscoelasticity of ion channels is adapted from [51] (the focus in [51] was to study mechanical deformations of a neuron with a healthy electric activity described by the classic Hodgkin-Huxley model exposed to traumatic mechanical events). The viscoelastic behavior of the channels is described by the variable-order fractional Maxwell linear viscoelastic model which was introduced in [52] without a detailed presentation of its properties. The Haar piecewise-constant approximants of the variable fractional orders are used to highlight the creep and relaxation properties of the chosen viscoelastic model. Lastly, using the fact that ACh acts upon the structure of the ligand-gated ion channels to facilitate action potentials and assuming that the concentrations of ACh and donepezil in a brain with AD treated with donepezil are proportional, the coupling of the two generalized models is achieved by taking the variable fractional order describing the viscoelastic fading memory of the ion channels to be dependent on the concentration of donepezil. Numerical simulations show the following: (1) in the brain, an anomalous release donepezil decays slower than a donepezil solution available on the market, (2) abnormal action potentials correspond to longer viscoelastic fading memory of the ion channels, and (3) donepezil intake temporarily recovers healthy action potentials which agrees with clinical observations [7].

Thus, the original contributions of this paper are:

1. a pharmacokinetic model showing that anomalous release modalities of donepezil can slow down the decay of the drug in the brain which may provide effective treatments for AD with smaller drug dosages;
2. an electromechanical model of ion channels showing that: (1) a shorter viscoelastic fading memory modulated by the ACh binding is associated with a properly functioning neuron, (2) a longer viscoelastic memory corresponding to ion channels structurally altered by AD progression causes abnormal action potentials, and (3) donepezil intake can recover the structural fitness of the ion channels as well as healthy action potentials by using anomalous release donepezil either combined or not with various drug dosages depending on the AD severity;
3. Haar piecewise-constant approximations can be used to characterize the creep and relaxation properties of the variable-order fractional Maxwell linear viscoelastic model assumed to describe the mechanical behavior of ion channels.

Figure 1 shows a schematic of this paper's main contributions (represented by blue, green and red fonts) and how they link to specific knowledge about AD and donepezil treatment that was mentioned earlier. It is hoped that this work may inspire future studies of the neuronal electromechanical properties in health and AD that could lead to improved personalized therapies for AD and other brain disorders.

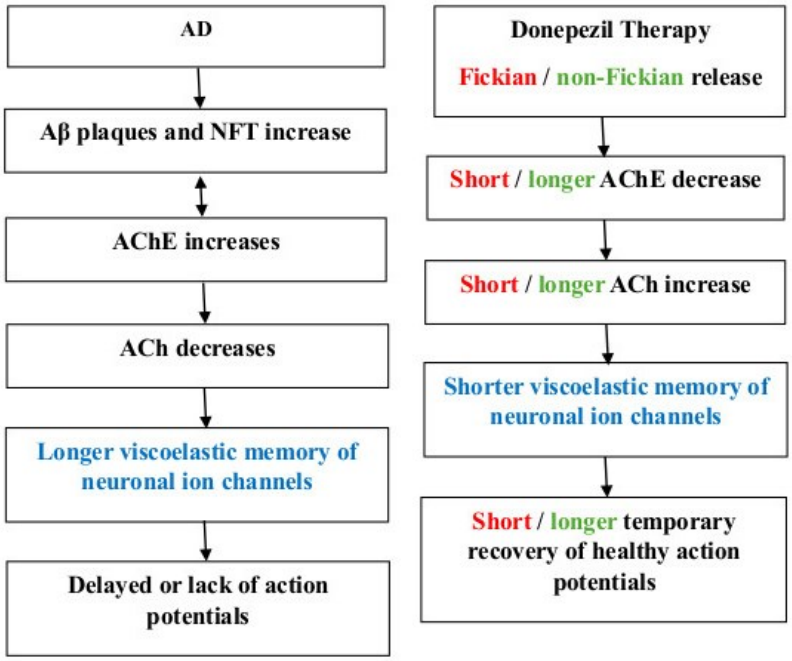

Figure 1. Schematics of simplistic linkages between AD/donepezil treatment and action potentials via the viscoelasticity of ion channels. The abnormal accumulations of $A\beta$ plaques and NFT specific to AD cause and benefit from an increase in the amount of AChE that leads to a decrease in the quantity of ACh available for binding to the nicotinic ACh receptors (and cholinergic ACh receptors, in general). The lack of ACh changes the structure of these receptors and their viscoelastic fading memory becomes longer which further causes delayed or loss of action potentials. On the other hand, donepezil treatment reduces temporarily the quantity of AChE and thus contributes to an increase in the amount of ACh. The binding between ACh and nicotinic ACh receptors changes the viscoelastic behavior of these receptors. The shorter fading memory modulated by the ACh binding leads to a temporary recovery of the healthy action potentials. Lastly, an anomalous release donepezil decays slower in the brain than a classic Fickian release, thus facilitating the propagation of healthy action potentials for a longer time. The blue, green and red fonts highlight this paper's main contributions.

The paper is organized as follows. A brief review of Caputo fractional derivatives of constant and variable orders and Haar wavelets is given in Section 2. Section 3 introduces the variable-order fractional Maxwell linear viscoelastic model, the generalized Hodgkin-Huxley and pharmacokinetic models and the coupling of these generalized models. Numerical results are shown in Section 4. Lastly, a discussion and concluding remarks are presented in Section 5.

2. Mathematical Preliminaries

The mathematical concepts needed in this paper are reviewed in this section. Readers familiar with these concepts may skip this section.

Definition 1. *1. [53] (p. 33), [54]: The* ***left-sided Riemann-Liouville fractional integral of constant order*** δ, $\delta > 0$, *of a function* $f \in L^1(a,b)$, $(a,b) \subset \mathbb{R}$, *is:*

$$I_{a+}^{\delta} f(x) = \frac{1}{\Gamma(\delta)} \int_a^x \frac{f(y)}{(x-y)^{1-\delta}} dy, \tag{1}$$

where $\Gamma(s) = \int_0^\infty t^{s-1}e^{-t}dt$ *is the gamma function. In particular,* $I_{a+}^0 f(x) = f(x)$.

2. *[54,55]: Let* $f : [a,b] \to \mathbb{R}$ *be a p-times differentiable function on* $(a,b) \subset \mathbb{R}$ *whose* p^{th}*-order derivative denoted by* $f^{(p)}$ *satisfies* $f^{(p)} \in L^1(a,b)$*, where* $p \in \{1,2,3,\dots\}$*. The* ***left-sided Caputo fractional derivative of constant order*** δ*,* $p-1 < \delta < p$*, of the function* f *is:*

$$D_{a+}^{\delta} f(x) = \frac{1}{\Gamma(p-\delta)} \int_a^x \frac{f^{(p)}(y)}{(x-y)^{\delta+1-p}} dy = I_{a+}^{p-\delta} f^{(p)}(x). \tag{2}$$

In particular, $D_{a+}^{p} f(x) = f^{(p)}(x)$.

3. *[56,57]: The* ***left-sided Caputo fractional derivative of variable order*** $\delta(x)$*,* $p-1 < \delta(x) < p$ *for* $p \in \{1,2,3,\dots\}$ *and* $x \in (a,b) \subset \mathbb{R}$ *of a function* $f : [a,b] \to \mathbb{R}$ *that is p-times differentiable on* (a,b) *and has* $f^{(p)} \in L^1(a,b)$ *is:*

$$D_{a+}^{\delta(x)} f(x) = \frac{1}{\Gamma(p-\delta(x))} \int_a^x \frac{f^{(p)}(y)}{(x-y)^{\delta(x)+1-p}} dy. \tag{3}$$

In [58], the variable-order Caputo fractional derivative (3) is called the variable order fractional derivative type 1.

Proposition 1. *1. [53] (p. 40), [54]: If* $\delta \in \mathbb{R}$ *and* $x > a$ *then:*

$$I_{a+}^{\delta}(x-a)^{\gamma-1} = \frac{\Gamma(\gamma)}{\Gamma(\delta+\gamma)}(x-a)^{\delta+\gamma-1},\ Re(\gamma) > 0, \tag{4}$$

$$D_{a+}^{\delta} c = 0,\ \forall c \in \mathbb{R}, \tag{5}$$

and, if $p-1 < \delta < p$ *for* $p \in \{1,2,3\dots\}$*:*

$$D_{a+}^{\delta}(x-a)^{\gamma-1} = \begin{cases} \frac{\Gamma(\gamma)}{\Gamma(\gamma-\delta)}(x-a)^{\gamma-\delta-1}, & \gamma > p,\ \gamma \in \mathbb{R}, \\ 0, & \gamma \in \{1,2,\dots,p\}. \end{cases} \tag{6}$$

2. *[54], [59] (p. 18): If* $p-1 < \delta \le p$ *for* $p \in \{1,2,3\dots\}$ *and* $f : [a,b] \to \mathbb{R}$ *is a p-times differentiable function such that there exist* $r > \gamma \ge -1$ *and a continuous function* $g : (a,b) \to \mathbb{R}$ *such that* $f^{(p)}(x) = x^r g(x)$ *for* $x > a$ *then*

$$\begin{aligned} D_{a+}^{\delta} I_{a+}^{\delta} f(x) &= f(x), \\ I_{a+}^{\delta} D_{a+}^{\delta} f(x) &= f(x) - \sum_{j=0}^{p-1} f^{(j)}(a+)\frac{x^j}{j!}. \end{aligned} \tag{7}$$

3. *[59] (pp. 4, 19), [50] (pp. 60, 222–229): If* f*,* $D_{0+}^{\delta} f \in L^1(0,+\infty)$*, for* $p-1 < \delta \le p$ *and* $p \in \{1,2,3\dots\}$*, then the following identity holds:*

$$\mathcal{L}\left[D_{0+}^{\delta} f\right](s) = s^{\delta}\mathcal{L}[f](s) - \sum_{k=0}^{p-1} s^{\delta-k-1} f^{(k)}(0+), \tag{8}$$

where $\mathcal{L}[f](s) = \int_0^\infty e^{-sx} f(x)dx$*,* $s \ge 0$ *is the Laplace transform of the function* f*. Also, for* $0 < \delta \le 1$*:*

$$\begin{aligned} \mathcal{L}\left[\frac{x^{-\delta}}{\Gamma(1-\delta)}\right](s) = s^{1-\delta},\ \mathcal{L}\left[\frac{x^{\delta}}{\Gamma(1+\delta)}\right](s) = \frac{1}{s^{1+\delta}}, \\ \mathcal{L}\left[E_{\delta}\left(-(x/a)^{\delta}\right)\right](s) = \frac{s^{\delta-1}}{s^{\delta}+(1/a)^{\delta}}, \end{aligned} \tag{9}$$

where $E_\delta(z) = \sum_{k=0}^{\infty} \frac{z^k}{\Gamma(k\delta+1)}$, $\delta > 0$, $z \in \mathbb{C}$ *is the Mittag-Leffler function. In particular,* $E_1(z) = \mathrm{e}^z$.

4. *[58]: Let* $f : [0,T] \to \mathbb{R}$ *be a differentiable function,* $\delta : [0,T] \to (0,1]$, *and* $0 = x_0 < x_1 < \cdots < x_{N-1} < x_N = T$ *be an equally-spaced discretization of the interval* $[0,T]$ *of constant step size* Δx. *Denote by* $f^k = f(x_k)$, $\delta^k = \delta(x_k)$ *for* $x_k = k\Delta x$ *and* $k \in \{0,1,2,\ldots,N\}$. *Then a finite difference scheme for the variable-order fractional derivative (3) is:*

$$D_{0+}^{\delta(t)} f^{k+1} = \frac{\Delta x^{-\delta^{k+1}}}{\Gamma(2-\delta^{k+1})} \sum_{j=0}^{k} \left((j+1)^{1-\delta^{k+1}} - j^{1-\delta^{k+1}} \right) \left(f^{k+1-j} - f^{k-j} \right) + \mathcal{O}(\Delta x), \tag{10}$$

for $k = 0,1,2,\ldots,N-1$.

Fractional order integrals and derivatives of other special functions can be found in [53] (pp. 173–174), [60].

First introduced by Haar in [61], Haar wavelets are well-localized oscillatory functions in $L^2(\mathbb{R})$ (they have finite energy) with zero mean (derived from an admissibility condition that establishes the decay pattern of the Fourier transforms of the wavelets) [62] that have been used successfully in various applications such as signal/image processing [63] and numerically solving integro-differential equations [64–68]. In this paper, piecewise-constant approximants of variable fractional orders will be found using Haar wavelets and properties of the constant-order Caputo fractional derivative (2) will be applied to gain some insights into the behavior of the variable-order Caputo fractional derivative (3).

Definition 2 ([62] (pp. 69–82)). *1. The function* $H : \mathbb{R} \to \mathbb{R}$ *given by:*

$$H(x) = \begin{cases} 1, & 0 \le x < \frac{1}{2} \\ -1, & \frac{1}{2} \le x \le 1 \\ 0, & \text{otherwise} \end{cases}$$

is called the ***Haar mother wavelet****.*

2. *The functions* $H_{j,k} : \mathbb{R} \to \mathbb{R}$, $j,k \in \mathbb{Z}$, *given by:*

$$H_{j,k}(x) = 2^{j/2} H(2^j x - k),$$

are called the ***Haar wavelets****. They are obtained from function* H *by dilation with parameter* $j \in \mathbb{Z}$ *and translation with parameter* $k \in \mathbb{Z}$.

3. *The functions* $\varphi : \mathbb{R} \to \mathbb{R}$ *given by:*

$$\varphi(x) = \chi_{[0,1)}(x) = \begin{cases} 1, & 0 \le x < 1 \\ 0, & \text{otherwise} \end{cases}$$

is called the ***Haar scaling function****. Also, the dilation and translation of function* φ *generate scaling functions* $\varphi_{j,k} : \mathbb{R} \to \mathbb{R}$, $j,k \in \mathbb{Z}$, *defined as:*

$$\varphi_{j,k}(x) = 2^{j/2} \varphi(2^j x - k).$$

Proposition 2 ([62] (pp. 69–82), [69] (ch. 12)). *1. The following identity holds:*

$$H(x) = \frac{1}{\sqrt{2}} \varphi_{1,0}(x) - \frac{1}{\sqrt{2}} \varphi_{1,1}(x), \ x \in \mathbb{R}.$$

2. *The sequence* $\{\varphi_{J,k}\}_{k\in\mathbb{Z}} \cup \{H_{j,k}\}_{j\geq J,j,k\in\mathbb{Z}}$, $\forall J \in \mathbb{Z}$ *is a complete orthonormal sequence (orthonormal basis) in* $L^2(\mathbb{R})$. *Thus, every function* $f \in L^2(\mathbb{R})$ *can be represented as:*

$$f(x) = \sum_{k=-\infty}^{+\infty} c_{J,k}\varphi_{J,k}(x) + \sum_{j=J}^{+\infty}\sum_{k=-\infty}^{+\infty} d_{j,k}H_{j,k}(x),\ \forall J \in \mathbb{Z} \tag{11}$$

where the wavelet coefficients of f *are* $c_{J,k} =< f, \varphi_{J,k} >_{L^2(\mathbb{R})}$, $d_{j,k} =< f, H_{j,k} >_{L^2(\mathbb{R})}$, *and the* L^2*-inner product of two functions* $f, g \in L^2(\mathbb{R})$ *is:*

$$< f, g >_{L^2(\mathbb{R})} = \int_{\mathbb{R}} f(x)g(x)dx.$$

Representation (11) is known as the discrete Haar wavelet transform.

3. *The* ***scale spaces*** $V_J = \overline{\text{span}\{\varphi_{J,k}\}_{k\in\mathbb{Z}}}^{\|.\|_{L^2(\mathbb{R})}}$, $J \in \mathbb{Z}$, *is a* ***multiresolution analysis****, i.e.,*

$$V_J \subset V_{J+1} \subset L^2(\mathbb{R}), \forall J \in \mathbb{Z}, \text{ and } \overline{\cup_{J\in\mathbb{Z}} V_J}^{\|.\|_{L^2(\mathbb{R})}} = L^2(\mathbb{R}).$$

The ***detail spaces*** $W_J = \overline{\text{span}\{H_{J,k}\}_{k\in\mathbb{Z}}}^{\|.\|_{L^2(\mathbb{R})}}$, $J \in \mathbb{Z}$, *satisfy the scale-step property:*

$$V_{J_2} = V_{J_1} \bigoplus \bigoplus_{j=J_1}^{J_2-1} W_j,\ \forall J_1, J_2 \in \mathbb{Z},\ J_1 < J_2.$$

Above, the L^2*-norm is* $\|f\|_{L^2(\mathbb{R})} = \sqrt{< f, f >_{L^2(\mathbb{R})}}$ *for* $f \in L^2(\mathbb{R})$.

Thus, for a function $f \in L^2(\mathbb{R})$ and a scale $J \in \mathbb{Z}$,

1. the scale functions act as low-pass filters providing a coarse, piecewise-constant approximation (first series of representation (11)):

$$f(x) = \sum_{k=-\infty}^{+\infty} c_{J,k}\varphi_{J,k}(x) \in V_J, \tag{12}$$

2. wavelets are band-pass filters providing the details of f as $\sum_{k=-\infty}^{+\infty} d_{J,k}H_{J,k}(x) \in W_J$ (second series of representation (11)).

Figures 2 and 3g–i show plots of Caputo fractional derivatives of the function $f(x) = x$ calculated using Formula (6). For a constant fractional order $\delta \in (0, 1]$, the fractional derivative becomes flatter as δ increases to 1 (Figure 2). Variable-order Caputo fractional derivatives of the function $f(x) = x$ are also calculated using the Haar piecewise-constant approximants of the following variable fractional orders: $\delta(x) = 0.25 + 0.15x$, $\delta(x) = 0.5 + 0.25\sin\frac{8x}{\pi}$, and $\delta(x) = 0.25 + 2e^{-x}$. Plots of the chosen variable orders and their corresponding Haar piecewise-constant approximants given by Formula (12) are shown in Figure 3a–f. The piecewise-constant approximants are found by applying the direct and inverse Haar wavelet transforms using Matlab's built-in functions **haart** and **ihaart** [70]. On each subinterval of a numerical discretization of the interval $[0, 5]$ the approximant is constant and Formula (6) can be used to calculate the corresponding constant-order Caputo fractional derivative. The plots in Figure 3g–i show not only that the variable-order Caputo fractional derivatives are bounded between the constant-order fractional derivatives for $\delta = 0.25$ and $\delta = 1$ since $\delta(x) \in (0.25, 1)$ for all considered cases, but also that certain features of the variable orders $\delta(x)$ seen in Figure 3a–c are transferred to the corresponding derivatives.

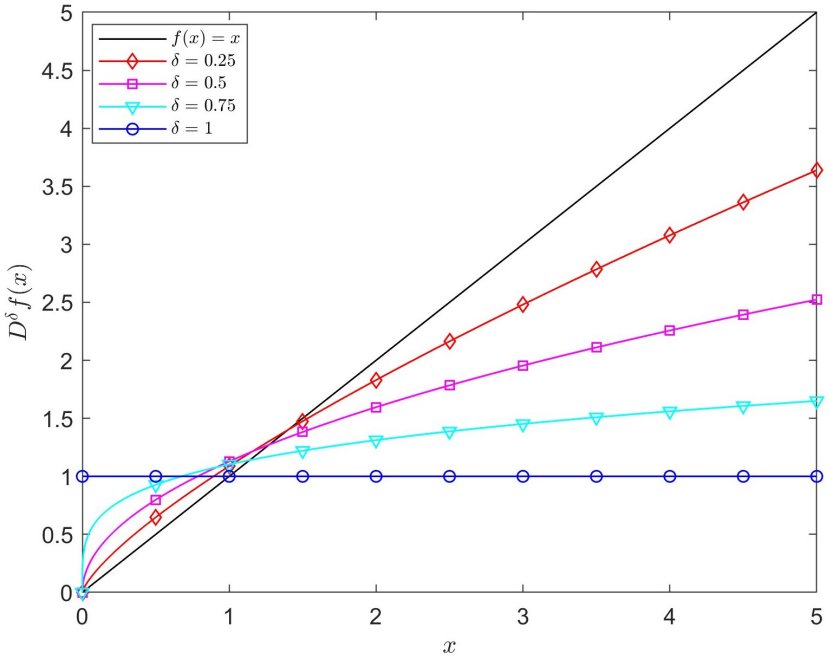

Figure 2. Plots of the function $f(x) = x$, $x \in [0, 5]$, and its constant-order Caputo fractional derivatives calculated for various constant fractional orders $\delta \in (0, 1]$.

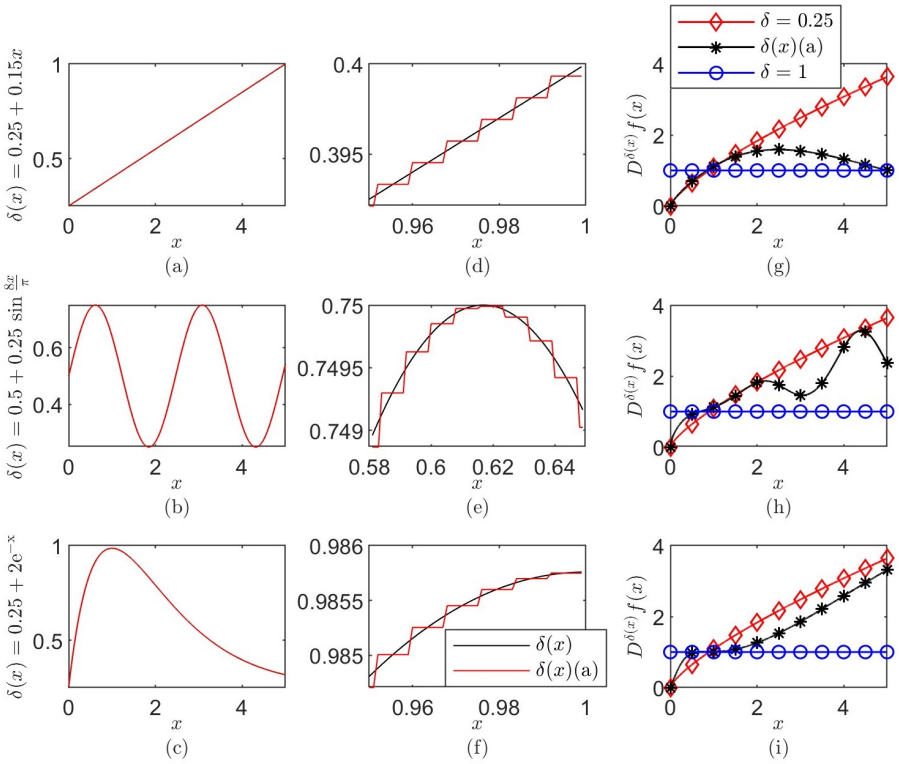

Figure 3. Plots of variable fractional orders $\delta(x)$ (black line) and their corresponding Haar piecewise-constant approximants (red line): (**a**) $\delta(x) = 0.25 + 0.15x$, (**b**) $\delta(x) = 0.5 + 0.25 \sin \frac{8x}{\pi}$, and (**c**) $\delta(x) = 0.25 + 2e^{-x}$. (**d**–**f**) Zoomed-in views of the plots shown in (**a**–**c**). (**g**–**i**) Plots of the variable-order Caputo fractional derivatives of the function $f(x) = x$, $x \in [0, 5]$, for the Haar piecewise-constant approximants of the variable orders plotted in (**a**–**c**). (**a**–**f**) share the legend located in (**f**), while (**g**–**i**) share the legend in (**g**). In the legend maps, (**a**) stands for the piecewise-constant approximant of $\delta(x)$.

In this paper it is assumed that $0 < \delta,\ \delta(x) \leq 1$. Then, the constant-order and variable-order Caputo fractional derivatives (2) and respectively (3) model fading memory, and the memory gets smaller as the fractional order approaches 1. Also, the variable-order fractional derivative (3) conserves physical causality [71] for continuous functions $f(x)$ and has no memory of its past order [72]. The lack of past order memory gives the derivative (3) the ability to transfer to the output specific features (such as monotonicity or oscillatory behavior) of the fractional order $\delta(x)$ [73].

Remark 1. *Fading memory is terminology commonly used in the theory of viscoelasticity. However, anomalous diffusion processes are described using the mathematical concepts and language of probability theory. The integro-differential representation with a slowly decreasing power law kernel of the Caputo fractional derivative has been linked to the long-tailed waiting time probability density function with an asymptotic inverse power law expression specific to anomalous diffusion [49].*

3. Mathematical Modeling

The model of a variable-order fractional Maxwell linear viscoelastic material introduced in Section 3.1 is used to describe the mechanical behavior of neuronal ion channels and the corresponding generalized Hodgkin-Huxley model is presented in Section 3.2. The transport of a controlled release donepezil through various compartments of the body is described by the generalized pharmacokinetic model presented in Section 3.3. Lastly, the coupling of the proposed generalized Hodgkin-Huxley and pharmacokinetic models is given in Section 3.4. Figure 4 shows how these subsections are linked. The descriptions and physical units of the models' variables are given in Table A1.

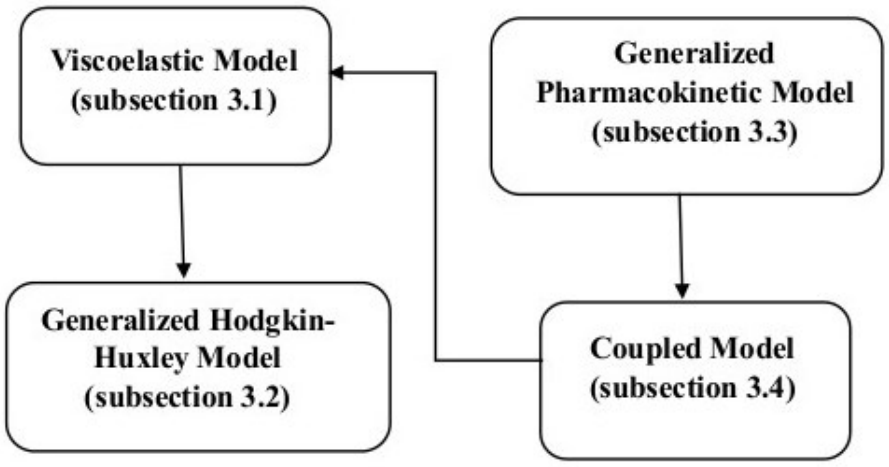

Figure 4. Linkages among Sections 3.1–3.4 of this section.

3.1. Viscoelastic Model

The constitutive equation of a variable-order fractional Maxwell linear viscoelastic model (schematically represented as an elastic spring connected in series to a viscous dashpot with long memory) is [52]:

$$D_{0+}^{\delta(t)}\sigma = E\left(D_{0+}^{\delta(t)}\epsilon - \frac{\sigma}{\mu_\delta}\right), \tag{13}$$

where $\sigma(t)$ and $\epsilon(t)$ are the stress and respectively infinitesimal strain in the one-dimensional case, and $t \geq 0$ denotes the physical time. The model has three physical parameters: E, the modulus of elasticity (of the spring element), μ_δ, and $0 < \delta(t) \leq 1$ (μ_δ, $\delta(t)$ correspond to the dashpot element). If $\delta(t) = \delta$ is a constant then Equation (13) becomes the fractional Maxwell model for $\delta \in (0, 1)$ [50] (p. 62), [74], or the classic Maxwell model for $\delta = 1$ [75] (pp. 53–55), [50] (p. 32). Also, in the case $\delta(t) = 1$, $\forall t \geq 0$, parameter μ_δ is the dynamic

viscosity μ and, thus, μ_δ is called the generalized viscosity. Lastly, the initial condition compatible with Equation (13) is the same as for the classic Maxwell model, namely:

$$\sigma(0+) = E\,\epsilon(0+). \tag{14}$$

If M, L, and T denote characteristic mass, length, and time, then dimensional analysis gives the dimensions of the physical quantities in Equation (13):

$$[\epsilon] = 1,\ [\delta(t)] = 1,\ [\sigma] = [E] = ML^{-1}T^{-2},\ [\mu_\delta] = ML^{-1}T^{\delta(t)-2} \tag{15}$$

since $\left[D_{0+}^{\delta(t)} f\right] = [f]T^{-\delta(t)}$ for a physical quantity f of dimension $[f]$.

When the variable fractional order is a constant $\delta \in (0, 1]$, then [50] (p. 62):

1. the creep compliance $J(t)$ is the strain per unit applied constant stress σ_0 calculated from Equation (13). By replacing $\sigma = \sigma_0$ in Equation (13), using Formula (5), and then applying the Laplace transform to the updated Equation (13) combined with $\sigma_0 = E\epsilon(0+)$ (Formula (14) corresponding to this case), the following expression for J can be obtained from Formulas (8) and (9):

$$J(t) = \frac{1}{E} + \frac{1}{\mu_\delta \Gamma(1+\delta)} t^\delta. \tag{16}$$

2. the relaxation modulus $G(t)$ is the stress per unit applied constant strain ϵ_0 calculated from Equation (13). By replacing $\epsilon = \epsilon_0$ in Equation (13), using Formula (5), and then applying the Laplace transform to the updated Equation (13) combined with $\sigma(0+) = E\epsilon_0$ (Formula (14) corresponding to this case), the following expression for G can be obtained from Formulas (8) and (9):

$$G(t) = E\,E_\delta\left(-\frac{E}{\mu_\delta} t^\delta\right). \tag{17}$$

In particular, if $\delta(t) = 1, \forall t \geq 0$, then the corresponding creep compliance and relaxation modulus can also be obtained as closed-form solutions of first order linear (and separable) ordinary differential equations derived from Equation (13) [75] (pp. 53–55):

$$J(t) = \frac{1}{E} + \frac{1}{\mu} t, \tag{18}$$

$$G(t) = E\,\mathrm{e}^{-\frac{E}{\mu}t}. \tag{19}$$

While Formula (18) is precisely Formula (16) for $\delta = 1$, Formula (19) admits a Taylor series representation given by Formula (17) for $\delta = 1$. In this case, Formula (17) approximates the function (19). Figure 5 shows plots of dimensionless functions $J(t)$ and $G(t)$ given by Formulas (16) and (17) versus a dimensionless time t for dimensionless parameters $E = 1$, $\mu_\delta = 1$ and various constant values of δ. The tail of the relaxation modulus gets longer as δ decreases to 0 (the decaying exponential behavior corresponding to $\delta = 1$ has the shortest tail; see Figure 5b).

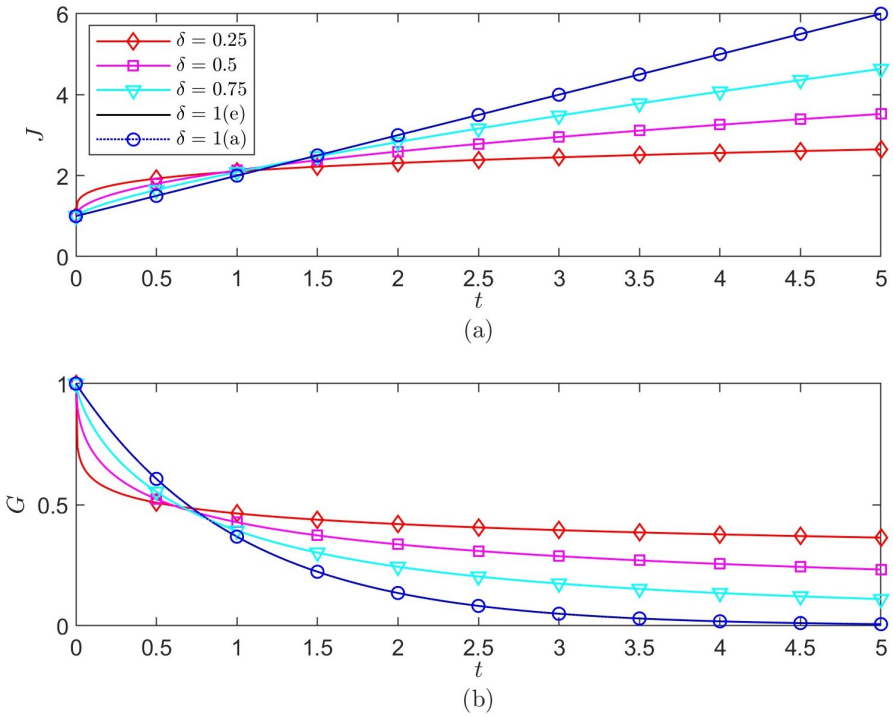

Figure 5. Plots of dimensionless (**a**) creep compliance $J(t)$ (Formula (16)) and (**b**) relaxation modulus $G(t)$ (Formula (17)) versus a dimensionless time t for dimensionless parameters $E = 1$, $\mu_\delta = 1$ and various constant fractional orders $\delta \in (0, 1]$. For $\delta = 1$, a perfect agreement is observed between the closed-form expressions (18), (19) (denoted by (e) in the legend) and the approximations (16), (17) (denoted by (a) in the legend). (**a**,**b**) share the legend in (**a**).

For a variable fractional order $\delta(t)$, the creep compliance and relaxation modulus are combinations of the creep and relaxation functions corresponding to multiple constant fractional orders. Indeed, if the variable fractional orders introduced in Section 2 and their corresponding Haar piecewise-constant approximants are used again, the creep compliance and relaxation modulus can be calculated using Formula (16) and respectively (17) on each subinterval of a numerical discretization of the chosen dimensionless time interval where the approximant is constant. The plots in Figure 6g–l, obtained for dimensionless parameters $E = 1$, $\mu_\delta = 1$, show that the approximated creep compliances and relaxation moduli corresponding to the given variable fractional orders $\delta(t)$ are bounded between the creep compliances and respectively relaxation moduli corresponding to the constant fractional orders $\delta = 0.25$ and $\delta = 1$ since $\delta(t) \in (0.25, 1)$ for all considered cases, and specific features of the variable orders $\delta(t)$ is transferred to the corresponding functions $J(t)$ and $G(t)$. For the sake of simplicity, plots of the chosen functions $\delta(t)$ and their corresponding piecewise-constant approximants are shown in Figure 6a–f. As expected from Formula (16), the approximated creep compliances corresponding to the variable fractional orders shown in Figure 6a–c resemble the plots in Figure 3g–i. For larger values of t, the relaxation modulus corresponding to the linear variable fractional order $\delta(t)$ plotted in Figure 6a decreases almost linearly (Figure 6j), while the tail of $G(t)$ plotted in Figure 6l becomes longer on the region where the variable fractional order $\delta(t)$ shown in Figure 6c experiences exponential decay. Lastly, the oscillatory decay of the relaxation modulus seen in Figure 6k is due to the oscillations of the variable fractional order $\delta(t)$ shown in Figure 6b.

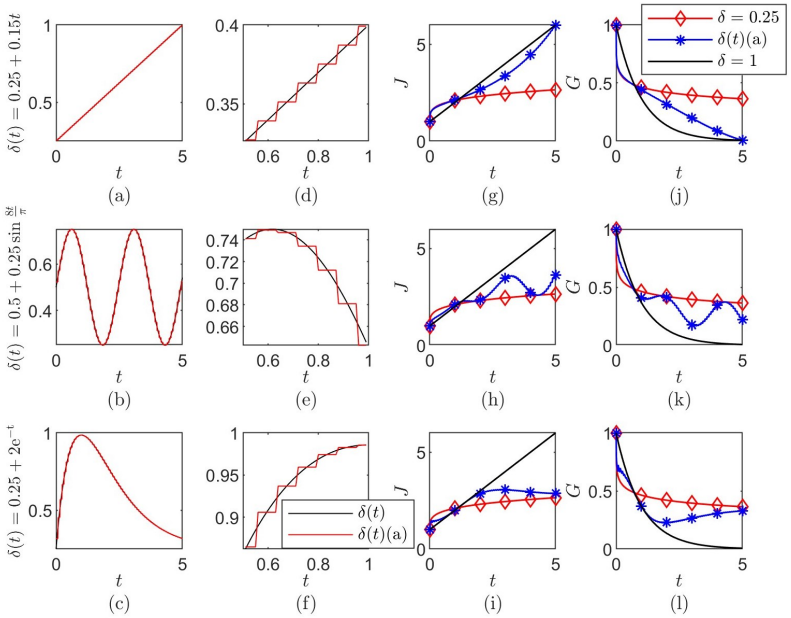

Figure 6. Plots of variable fractional orders $\delta(t)$ (black line) and their corresponding Haar piecewise-constant approximants (red line): (**a**) $\delta(t) = 0.25 + 0.15t$, (**b**) $\delta(t) = 0.5 + 0.25\sin\frac{8t}{\pi}$, and (**c**) $\delta(t) = 0.25 + 2e^{-t}$. (**d**–**f**) Zoomed-in views of the plots shown in (**a**–**c**). (**g**–**i**) Plots of dimensionless creep compliance $J(t)$ versus a dimensionless time t for dimensionless parameters $E = 1$, $\mu_\delta = 1$ and the Haar piecewise-constant approximants of the variable orders plotted in (**a**–**c**). (**j**–**l**) Plots of dimensionless relaxation modulus $G(t)$ versus a dimensionless time t for dimensionless parameters $E = 1$, $\mu_\delta = 1$ and and the Haar piecewise-constant approximants of the variable orders plotted in (**a**–**c**). (**a**–**f**) share the legend located in (**f**), while (**g**–**l**) share the legend in (**j**). In the legend maps, (**a**) stands for the piecewise-constant approximant of $\delta(t)$.

Since a variable fractional order $\delta(t)$ admits a Haar piecewise-constant approximant and the creep compliance $J(t)$ and relaxation modulus $G(t)$ corresponding to a constant fractional order are given by power law expressions (16) and respectively (17), the dimensionless physical parameter $\delta(t)$ of model (13) can be called the memory parameter.

Remark 2. *By using a Haar piecewise-constant approximation (12) of the memory parameter $\delta(t)$, definition (1) and property (7) of fractional calculus, and the initial condition (14), it can be shown that the constitutive law (13) can be written as a linear relationship between the stress $\sigma(t)$ and strain $\epsilon(t)$ involving a single integral with a power law memory kernel. For infinitesimal deformations, this one integral representation of the constitutive law can also be derived via the linearization of the Pipkin-Rogers model of non-linear viscoelasticity [76] that uses the Fréchet approximation of continuous functionals proposed in [77] to represent the stress as an infinite sum of multiple integrals of the finite strain-rate histories (also called a Volterra series, see [78]) whose so-called memory kernels are positive, at least continuous and monotonic decreasing functions of time so that they model viscoelastic fading memory. For model (13), the memory kernel is chosen to be a power law.*

3.2. Generalized Hodgkin-Huxley Model

In [51], a Lagrangian formulation and Hamilton's principle are used to derive the coupled equations describing neuronal electromechanics. The three ion gates m, n, and h whose open or close states produce action potentials in the classic Hodgkin-Huxley model [42] are assumed to behave mechanically like variable-order fractional Maxwell linear viscoelastic materials of constitutive Equation (13). Thus, in this context, m, n, and h, that in the Hodgkin-Huxley model are variables representing the activations of the Na^+ and K^+ channels and the inactivation of the Na^+ channel, respectively, become nondimensional displacements of the dashpots in the Maxwell elements modeling the material structures

of the ion channels. The equations of the generalized Hodgkin-Huxley model link the electric activity of a neuronal membrane and the viscoelastic behavior of the membrane's ion channels as follows (these equations have simpler expressions than those in [51] since the neuronal mechanical behavior is neglected here; also, in [51], the focus was on the effects of traumatic mechanical events on neuronal deformation and thus only the classic Hodgkin-Huxley model was used in the numerical simulations):

$$c_m V^{(1)} = I - \left(G_{Na} m^3 h + G_{NaL}\right)(V - E_{Na}) - \left(G_K n^4 + G_{KL}\right)(V - E_K) - G_{ClL}(V - E_{Cl}), \tag{20}$$

$$D_{0+}^{\delta(t)} m = \alpha_m (1 - m) - \beta_m m, \tag{21}$$

$$D_{0+}^{\delta(t)} n = \alpha_n (1 - n) - \beta_n n, \tag{22}$$

$$D_{0+}^{\delta(t)} h = \alpha_h (1 - h) - \beta_h h, \tag{23}$$

with initial conditions:

$$V(0) = V_{\text{rest}},\ m(0) = \frac{\alpha_m(V(0))}{\alpha_m(V(0)) + \beta_m(V(0))},$$
$$n(0) = \frac{\alpha_n(V(0))}{\alpha_n(V(0)) + \beta_n(V(0))},\ h(0) = \frac{\alpha_h(V(0))}{\alpha_h(V(0)) + \beta_h(V(0))}, \tag{24}$$

where:

$$\alpha_m = \frac{0.32(V + 54)}{1 - \mathrm{e}^{-0.25(V+54)}},\ \beta_m = \frac{0.28(V + 27)}{\mathrm{e}^{0.2(V+27)} - 1},$$
$$\alpha_n = \frac{0.032(V + 52)}{1 - \mathrm{e}^{-0.2(V+52)}},\ \beta_n = 0.5\mathrm{e}^{-(V+57)/40},$$
$$\alpha_h = 0.128\mathrm{e}^{-(V+50)/18},\ \beta_h = \frac{4}{1 + \mathrm{e}^{-0.2(V+27)}}. \tag{25}$$

In Equation (20), c_m is the specific membrane capacitance, I is an externally applied current per unit area, E_{Na}, E_K, and E_{Cl} are the reverse potentials, and G_{Na}, G_K, G_{NaL}, G_{KL}, and G_{ClL} are, respectively, the voltage-gated maximal conductances of Na^+ and K^+, and the leak conductances of Na^+, K^+, and Cl^-. The membrane potential and its first order derivative are denoted by $V(t)$ and $V^{(1)}(t)$, respectively. The resting membrane potential is V_{rest}. The values of the physical parameters in Equations (20)–(23) are given in Table 1. These values are assumed to correspond to a properly functioning neuron.

Table 1. The values, physical units and descriptions of the model's parameters.

Parameters	Values and Physical Units [Reference]	Description
V_{rest}	−65 mV [43]	Normal resting potential
E_{Na}	60 mV [43]	Reversal potential of persistent sodium current
E_K	−88 mV [43]	Reversal potential of potassium current
E_{Cl}	−61 mV [43]	Reversal potential of chloride current
G_{Na}	0.3 mS/mm^2 [43]	Maximal conductance of sodium current
G_K	0.25 mS/mm^2 [43]	Maximal conductance of potassium current
G_{NaL}	0.000247 mS/mm^2 [43]	Conductance of leak sodium current
G_{KL}	0.0005 mS/mm^2 [43]	Conductance of leak potassium current
G_{ClL}	0.001 mS/mm^2 [43]	Conductance of leak chloride current
c_m	0.01 μF/mm^2 [43]	Membrane capacitance
I	0.1 μA/mm^2 [43]	Applied current

Like in the classic Hodgkin-Huxley model, Equation (20) represents Kirchhoff's current law. However, Equations (21)–(23) represent now evolution equations for the nondimensional displacements of the m, n, and h gates. In the classic Hodgkin-Huxley model,

Equations (21)–(23) were derived ad hoc from curve fitting to experiments and not from first principles. Also, given that there are no published experimental characterizations of the ion channels' viscoelasticity, it is assumed, for simplicity, that the viscoelastic fading memories of the ion channels are described by the same memory parameter $\delta(t)$. It is, however, possible to use different memory parameters in Equations (21)–(23) to model distinct patterns of viscoelastic fading memories of the channels. Furthermore, it is important to notice that this electromechanical model (20)–(23) can describe structurally intact as well as damaged neuronal membranes and thus predict various patterns of structurally dependent action potentials corresponding to both functional and dysfunctional neurons for the same externally applied current I and, for now, constant intra- and extra-cellular ion concentrations.

Lastly, the physical units of the parameters given by Formula (25) should be the same as those of the left-hand sides of the Equations (21)–(23), and thus all the constants multiplying potential V are meant to remove its physical units (mV). Furthermore, based on Formula (15) and the work in [51], these parameters have the following dimensions:

$$[\alpha_o] = [\beta_o] = \frac{[E_o]}{[\mu_{\delta_o}]} = T^{-\delta(t)}, \tag{26}$$

where $o \in \{m, n, h\}$ and E_o, μ_{δ_o} are the modulus of elasticity and, respectively, generalized viscosity of ion gate o. Formula (26) shows that the memory parameter $\delta(t)$ is intrinsic to the relaxation of the ion gates, which agrees with Formula (17) in the case of a constant fractional order δ. Thus, the relaxation time of ion gate o is given by $(\alpha_o + \beta_o)^{-1/\delta(t)}$.

3.3. Generalized Pharmacokinetic Model

In this paper the pharmacokinetic model of donepezil transport found in [32] is combined with the results on controlled release donepezil in [31]. In [32] mice received a donepezil solution orally and then the donepezil amounts were extracted from homogenized serum and brain tissue samples collected from the mice. By fitting the data to compartmental pharmacokinetic models using the software NONMEM 7.4 (NONlinear Mixed Effects Modeling), a three-compartment model that best describes the data was found. The compartments are: a depot for drug storage and distribution which for orally administered drugs is the stomach, the blood compartment, the brain, and the peripheral compartment. In [31], donepezil hydrochloride-encapsulated sodium alginate microspheres for oral administration are prepared. The controlled release of donepezil in vitro from the microspheres was fitted to a power law model. The exponent of release depended on the cross-linker concentration and time and suggested either a Fickian release pattern if its value was less than or equal to 0.5, or a non-Fickian (anomalous) diffusion pattern if the value was strictly greater than 0.5 and less than 1.

Following [49], in this paper anomalous diffusion will be modeled using a temporal Caputo fractional derivative of constant order $\varepsilon \in (0, 1)$ and, thus, the generalized pharmacokinetic model describing the transport to the brain of controlled release donepezil is:

$$\begin{aligned}
D^{\varepsilon}_{0+} c_d(t) &= -k_{12}\, c_d(t), \\
D^{\varepsilon}_{0+} c_{\text{blood}}(t) &= k_{12}\, c_d(t) - (k_{20} + k_{23} + k_{24})\, c_{\text{blood}}(t) + k_{42}\, c_p(t), \\
D^{\varepsilon}_{0+} c_{\text{brain}}(t) &= \frac{V_{\text{blood}}}{V_{\text{brain}}}\, k_{23}\, c_{\text{blood}}(t) - k_{30}\, c_{\text{brain}}(t), \\
D^{\varepsilon}_{0+} c_p(t) &= k_{24}\, c_{\text{blood}}(t) - k_{42}\, c_p(t),
\end{aligned} \tag{27}$$

where $0 < \varepsilon \leq 1$ is the dimensionless exponent of drug release, and c_d, c_{blood}, c_{brain}, and c_p are the drug's (mass) concentrations in the depot, blood, brain, and peripheral compartments, respectively. The case $\varepsilon = 1$ describes classic Fickian diffusion and also corresponds to the donepezil solution available on the market that was used in [32].

Parameter k_{12} gives the drug's absorption rate through the depot to the blood, and parameters k_{20} and k_{30} are drug's elimination rates due to biochemical processes taking place within the blood and brain, respectively. Parameters k_{23}, k_{24}, and k_{42} are drug's transfer rates from the blood to the brain, and, respectively, between the blood and peripheral compartments. The drug's production rate in the brain is rescaled because the volumes of drug distribution in the brain, V_{brain}, and in the blood, V_{blood} are different [32]. The values of these parameters are assumed to be the same as those found using data fitting in [32] and are given in Table 2. A dimensional analysis of system (27) finds the dimension of the rates in system (27) to be $T^{-\varepsilon}$ which explains the physical units in Table 2.

Table 2. The values, physical units and descriptions of the model's parameters.

Parameters	Values and Physical Units [Reference]	Description
k_{12}	$0.059\,\text{min}^{-\varepsilon}$ [32]	Absorption rate through the depot
k_{20}	$0.012\,\text{min}^{-\varepsilon}$ [32]	Elimination rate in the blood
k_{23}	$0.014\,\text{min}^{-\varepsilon}$ [32]	Transfer rate from blood to brain
k_{24}	$0.034\,\text{min}^{-\varepsilon}$ [32]	Transfer rate from blood to periphery
k_{42}	$0.011\,\text{min}^{-\varepsilon}$ [32]	Transfer rate from periphery to blood
k_{30}	$0.325\,\text{min}^{-\varepsilon}$ [32]	Elimination rate in the brain
V_{blood}	279 mL [32]	Volume of distribution in blood
V_{brain}	18 mL [32]	Volume of distribution in brain
ε	$\{0.5, 0.658, 0.868, 1\}$ [31,32]	Exponent of release

Since system (27) is linear, and the eigenvalues of the system's matrix with the values in Table 2 are real numbers, the analytic solution exists and is given by [79,80]:

$$\begin{pmatrix} c_d \\ c_{\text{blood}} \\ c_{\text{brain}} \\ c_p \end{pmatrix}(t) = \sum_{i=1}^{4} c_i\, \mathbf{v}_i\, E_\varepsilon(\lambda_i\, t^\varepsilon), \tag{28}$$

where λ_i, $i \in \{1,2,3,4\}$ are the eigenvalues of the system's matrix, $\mathbf{v}_i$, $i \in \{1,2,3,4\}$ are the corresponding eigenvectors, and c_i, $i \in \{1,2,3,4\}$ are constants of integration. The constants of integration are found from the following initial condition taken from [32]:

$$\begin{pmatrix} c_d \\ c_{\text{blood}} \\ c_{\text{brain}} \\ c_p \end{pmatrix}(0) = \begin{pmatrix} 0.89\,\frac{\mu\text{g}}{\text{mL}} \\ 0 \\ 0 \\ 0 \end{pmatrix}. \tag{29}$$

which is calculated from an orally administered donepezil dose of 250 µg.

3.4. Coupled Model

Nicotinic ACh receptors are large transmembrane proteins with complex structures made of long twisted and folded chains of amino acids [47,48] that resemble the microstructures of viscoelastic materials [81] (incidentally, voltage-gated ion channels have comparable structures and, thus, also exhibit viscoelastic behavior [82]). Since nicotinic ACh receptors and collagen molecules are polymers (with different internal conformations) and collagen molecules exhibit viscoelastic behavior [83], it is assumed that nicotinic ACh receptors are also viscoelastic materials, and their electro-mechanic response is described by the generalized Hodgkin-Huxley model. The binding of ACh molecules to nicotinic ACh receptors briefly changes the internal conformations of the receptors' structures to create transmembrane pores for the transport of ions across the neuronal membrane (action potentials). This fast structural rearrangement modulated by the ACh ligand can be modeled as a short viscoelastic fading memory. Thus, it can be assumed that the ligand-gated ion channels (and, based on [82], neuronal ion channels in general) are viscoelastic materials

with short viscoelastic memory such that they produce healthy action potentials that define a properly functioning neuron.

As mentioned in the introduction, the binding between AChE and donepezil increases the amount of ACh in the brain. In this paper it is assumed that the amount of donepezil in a brain with AD is proportional to the concentration of ACh and the following formula is proposed to model donepezil's effects on the viscoelastic behavior of the ligand-gated ion channels:

$$\delta(t) = \delta_{AD} + c_{\text{brain}}(t), \tag{30}$$

where $\delta_{AD} \in (0,1)$ is a constant for the AD-specific longer viscoelastic fading memory of the ligand-gated ion channels that causes abnormal action potentials (see later) and, by an abuse of notation, c_{brain} represents a nondimensional and rescaled concentration of donepezil in the brain calculated from Formula (28) such that $\delta(t) \in (0,1]$. Formula (30) that couples the generalized Hodgkin-Huxley and pharmacokinetic models presented earlier was chosen merely due to its mathematical simplicity since, currently, there are no published experimental observations supporting this formula.

Remark 3. *The extensions of the Picard-Lindeloff method proposed in [84,85] can be used to prove the existence and uniqueness of solutions to systems (20)–(23) and respectively (27) for constant fractional orders δ, $\varepsilon \in (0,1]$. Also, the extension of the method of Green's functions presented in [79] can be used to prove the existence of a unique solution of the system of linear fractional differential Equations (27). For a variable fractional order $\delta(t) \in (0,1]$, the Haar piecewise-constant approximant (12) of $\delta(t)$ can be used in combination with the extensions of the Picard-Lindeloff method in [84,85] to straightforwardly prove the existence and uniqueness of the solution of system (20)–(23).*

4. Results

This section presents numerical simulations obtained in Matlab [70]. Matlab's built-in function **ode15s** (implementation of variable-step, variable-order numerical differentiation formulas of orders 1 to 5) is used to numerically solve system (20)–(23) for $\delta = 1$, and Matlab's built-in function **ode45** (implementation of a single-step explicit Runge-Kutta (4,5) formula) is used to solve system (27) for $\varepsilon = 1$ [86]. For constant fractional orders δ, $\varepsilon \in (0,1)$, systems (20)–(23) and, respectively, (27) are solved numerically using Matlab's function **fde_pi1_ex** that implements the explicit product-integration rule of rectangular type with convergence order equal to one [87]. For a variable fractional order $\delta(t)$ given by Formula (30), system (20)–(23) is solved using the explicit Euler numerical scheme for Equation (20) and numerical scheme (10) for Equations (21)–(23) implemented in Matlab.

4.1. Action Potentials in Health and AD

Figures 7 and 8 show plots of the solutions of system (20)–(23) with initial conditions (24), parameters given by Formula (25) and in Table 1, and various constant fractional orders $\delta \in (0,1]$. Numerical solutions were obtained using the step size $\Delta t = 0.00025$ ms. The case $\delta = 1$ corresponds to the classic Hodgkin-Huxley model which is considered the healthy case (Figure 7a,e). It is assumed that the healthy action potentials are characterized by positive overshoots and ability to reach the value of the resting membrane potential given in Table 1. As δ decreases to 0, the viscoelastic memory of the ion gates gets longer slowing down the opening or closing of the m, n, and h gates (Figure 8). This causes the oscillations of the membrane's potential to become delayed (Figure 7b,c,e) and eventually cease to exist (Figure 7d,e). The amplitude of these oscillations also decreases with decreasing δ, and the positive overshoot stops to happen (Figure 7). Lastly, as δ gets smaller, the peak-to-peak amplitude of the membrane's potential gets shorter and the membrane potential does not reach the resting potential V_{rest} given in Table 1 anymore.

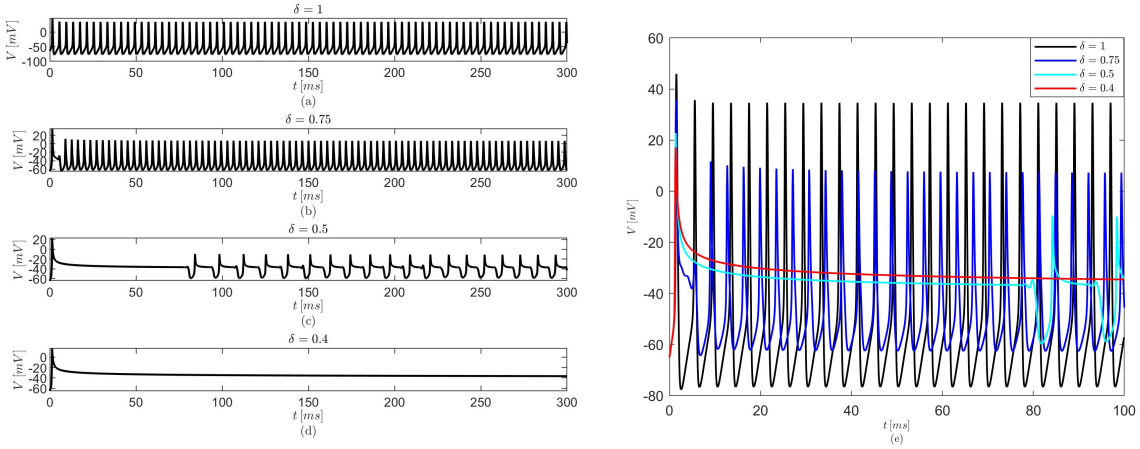

Figure 7. (**a**–**d**) Plots of membrane potentials for various constant fractional orders $\delta \in (0, 1]$. (**e**) A comparison of zoomed-in views of the plots shown in (**a**–**d**). As δ decreases to 0, the viscoelastic memory gets longer causing the peak-to-peak amplitude of the action potential V to get shorter and the resting potential to get higher. Also, plateau (delayed) potentials followed by higher frequency of firing are observed for $\delta = 0.75$, while for $\delta = 0.5$ a first long plateau region is followed by periodic shorter delayed potentials. Lastly, the action potentials cease to exist for values of δ closer to 0.

It is further assumed that a shorter viscoelastic memory (δ closer to 1) describes structurally intact ion gates that generate healthy action potentials and thus this neuron is considered functional. A longer viscoelastic memory (δ closer to 0) describes structurally altered ion gates assumed here to be caused by the decreased amount of ACh due to AD that generates abnormal action potentials and thus this is a dysfunctional neuron. It is also assumed that the abnormal action potentials for $\delta_{AD} = 0.75$ correspond to earlier stages of AD, and the abnormal action potentials for $\delta_{AD} = 0.5$ correspond to later stages of AD.

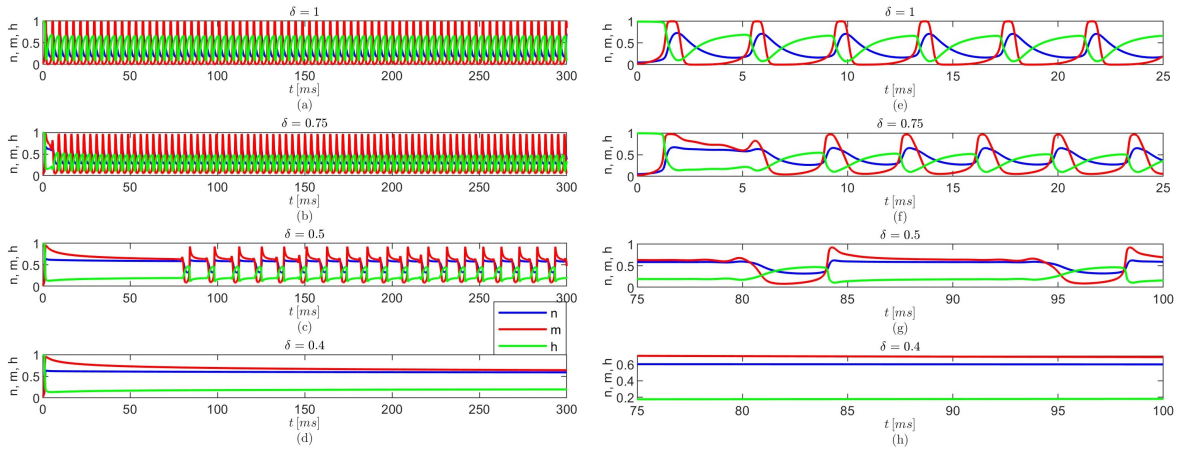

Figure 8. (**a**–**d**) Plots of displacements m, n, and h for various constant fractional orders $\delta \in (0, 1]$. (**e**–**h**) Zoomed-in views of the plots shown in (**a**–**d**). (**a**–**h**) share the legend in (**d**). As δ goes to 0, the periodic oscillations of m, n, and h gates start changing their shapes, plateau regions appear and get longer until the gates stop opening or closing.

4.2. Transport of Controlled Release Donepezil

Figures 9 and 10 show the solutions of system (27) with initial conditions (29) and parameters given in Table 2. The numerical solutions are obtained for a step size of $\Delta t = 0.005$ min. For each value of $\varepsilon \in (0, 1]$, a perfect agreement between the the analytic solution (28) and the numerical solution of system (27) is observed (Figure 9). This validates the numerical solutions obtained using Matlab's functions **fde_pi1_ex** and **ode45**. A comparison of the concentrations of donepezil for various value of ε in each of the

four compartments is shown in Figure 10. As ε decreases from 1, the concentration of controlled release donepezil gets longer tails at later times (Figure 10a–c). Since the very slow decay of donepezil in the stomach for $\varepsilon = 0.5$ may elevate gastrointestinal adverse effects (Figure 10a), the value $\varepsilon = 0.658$ is chosen as the optimal controlled release based on the slow decrease of donepezil in the brain (Figure 10c).

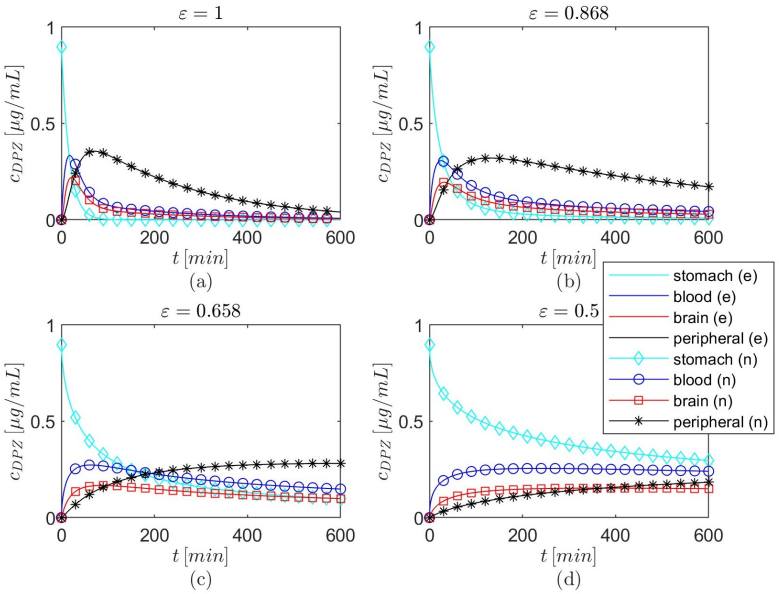

Figure 9. Plots of concentrations of donepezil in the depot, blood, brain and peripheral compartments for various constant values of ε. (**a**–**d**) share the legend in (**d**). In the legend map, (n) stands for numerical solution and (e) for exact (analytic) solution. The subscript DPZ stands for donepezil. For each value of ε, a perfect agreement is noticed between the exact and numerical solutions for each compartment.

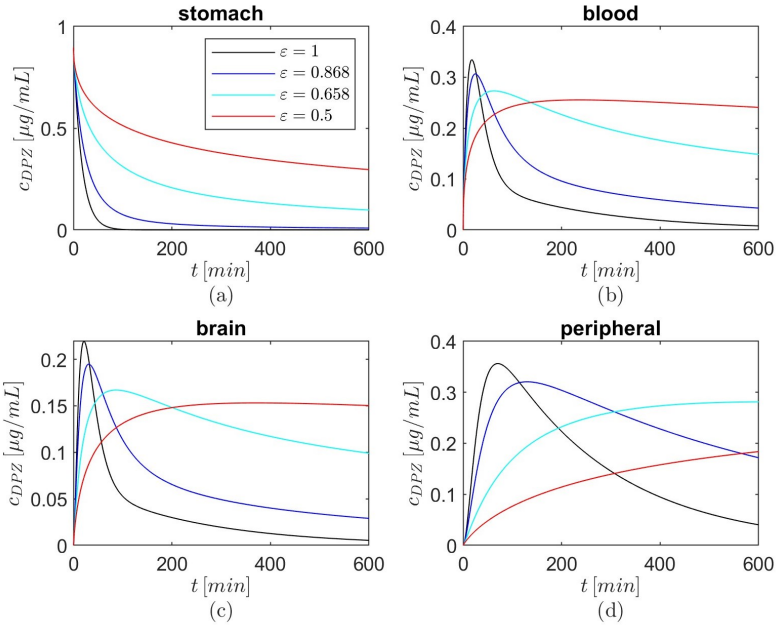

Figure 10. A comparison of concentrations of donepezil for various values of ε in each compartment: (**a**) depot, (**b**) blood, (**c**) brain, and (**d**) peripheral. The subscript DPZ stands for donepezil. The tail of the concentration in each compartment gets longer as ε decreases. Specifically, in the brain, as ε decreases, the maximum concentration of donepezil decreases and is reached at a later time, and the concentration decays slower with time.

4.3. Donepezil Effects on Action Potentials

Figure 11 shows plots of viscoelastic memories $\delta(t)$ given by Formula (30) for $\delta_{AD} \in \{0.5, 0.75\}$ and dimensionless and rescaled concentrations of controlled release donepezil in brain given by Formula (28) for $\varepsilon \in \{0.658, 1\}$. For $\delta_{AD} = 0.5$, the following cases are also considered: (1) the initially administered donepezil dose for $\varepsilon = 0.658$ is doubled to 500 μg, (2) the donepezil dosage is 250 μg every 120 min during the observed period of 600 min for $\varepsilon \in \{0.658, 1\}$. The concentrations of donepezil in brain are rescaled by interpolating using Matlab's built-in function **interp1** (Figure 11). It is further assumed that the shapes of the concentrations remain the same on a time scale of ms. This assumption allows to numerically solve system (20)–(23) for a variable fractional order $\delta(t)$ without exceeding Matlab's maximum array size and memory allowed by the computer used for calculations (HP Spectre 360× laptop with 64×-based PC and 8 GB RAM), and, thus, the patterns of the action potentials corresponding to the various shapes of $\delta(t)$ shown in Figure 11 can be visualized. The plots in Figure 11 resemble the variable fractional orders in Figure 6b,c so the creep and relaxation responses of viscoelastic materials with memories shown in Figure 11 will look like those in Figure 6h,k and respectively Figure 6i,l.

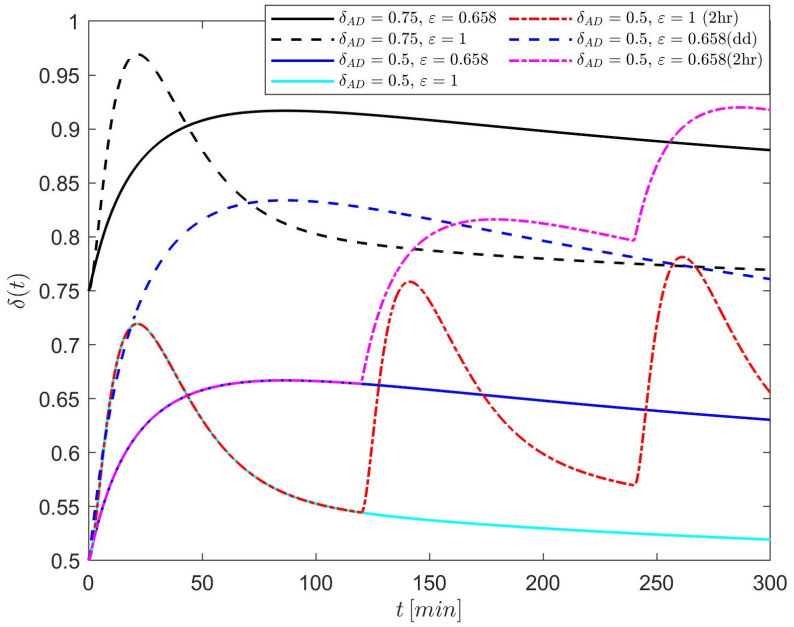

Figure 11. Plots of $\delta(t)$ given by Formula (30) for $\delta_{AD} \in \{0.5, 0.75\}$ and $\varepsilon \in \{0.658, 1\}$. In the legend map, (dd) stands for double dose, and (2 h) stands for the administration of donepezil every two hours. Due to computer memory constraints, it is assumed that the shapes of $\delta(t)$ remain unchanged on the time domain $[0, 300]$ ms of the membrane potential.

Figures 12–17 show plots of the solutions to system (20)–(23) with initial conditions (24), parameters given by Formula (25) and in Table 1 and variable fractional orders shown in Figure 11. The solutions are obtained for a step size $\Delta t = 0.005$ ms. The plots show the effects of controlled release donepezil on action potentials.

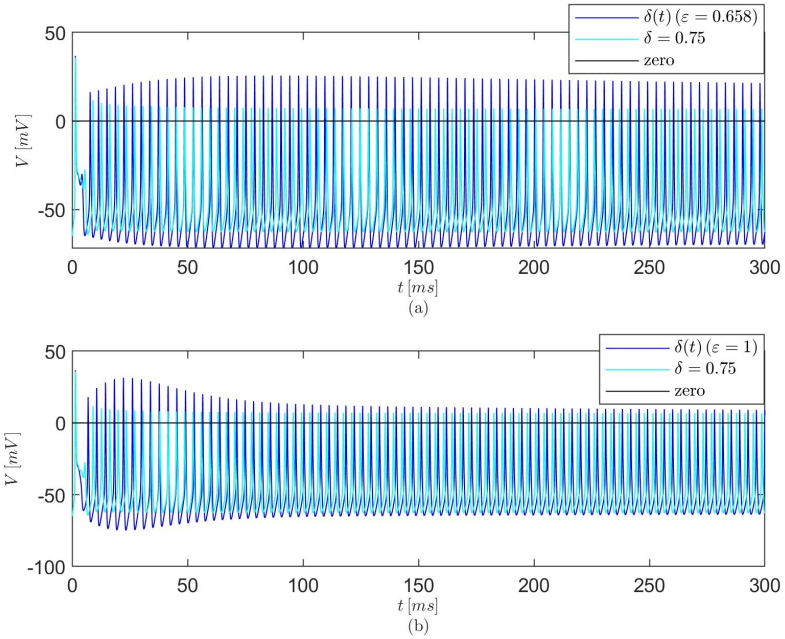

Figure 12. Action potentials for viscoelastic memories $\delta_{AD} = 0.75$ and, respectively, $\delta(t)$ given by Formula (30) with $\delta_{AD} = 0.75$ and controlled release donepezil for (**a**) $\varepsilon = 0.658$ and (**b**) $\varepsilon = 1$. Plots not to scale. Donepezil intake recovers the ability of the membrane potential to have positive overshoots and reach the normal resting potential for both values of ε.

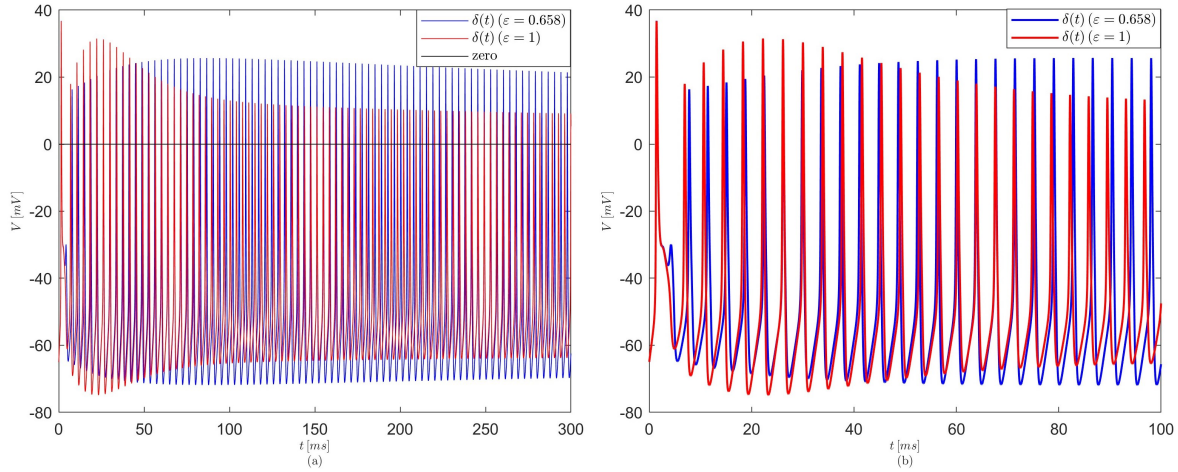

Figure 13. (**a**) Comparison of action potentials for viscoelastic memory $\delta(t)$ given by Formula (30) with $\delta_{AD} = 0.75$ and with Fickian ($\varepsilon = 1$) and non-Fickian ($\varepsilon = 0.658$) release of donepezil. (**b**) Zoomed-in view of the plots in (**a**). Plots not to scale. The membrane potential after donepezil treatment with non-Fickian control release has positive overshoots and reach the normal resting potential for a longer time and the peak-to-peak amplitude of the oscillations are larger than the membrane potential after donepezil intake with Fickian control release.

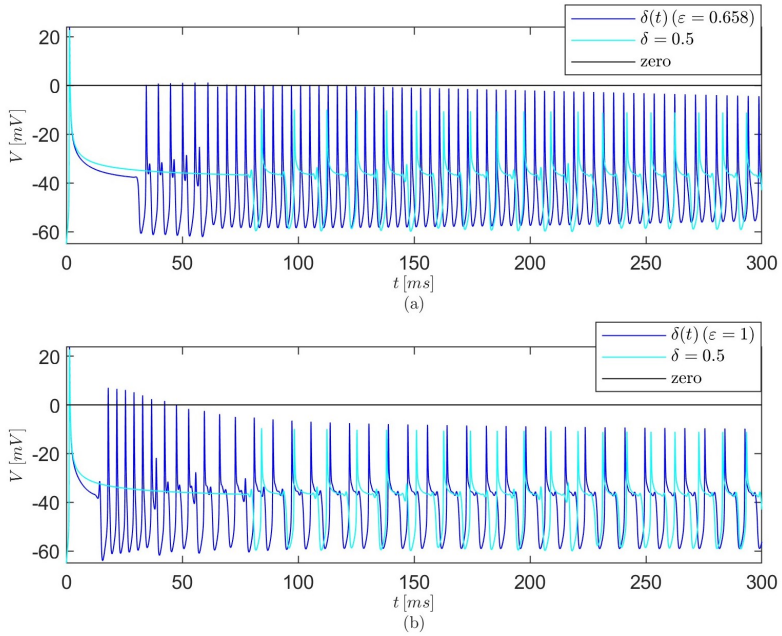

Figure 14. Action potentials for viscoelastic memories $\delta_{AD} = 0.5$ and, respectively, $\delta(t)$ given by Formula (30) with $\delta_{AD} = 0.5$ and with controlled release donepezil for (**a**) $\varepsilon = 0.658$ and (**b**) $\varepsilon = 1$. Plots not to scale. For a short time, donepezil intake recovers the ability of the membrane potential to have positive overshoots for $\varepsilon = 1$ and reach the normal resting potential for both values of ε. Also, the first plateau regions of the action potentials after donepezil treatment are shorter than the first plateau region of the potential corresponding to $\delta_{AD} = 0.5$. At later times, the action potentials corresponding to a donepezil treatment with $\varepsilon = 1$ develop shapes with small delays similar to those seen in the action potentials for the case $\delta_{AD} = 0.5$, while the action potentials associated with a donepezil intake with $\varepsilon = 0.658$ do not develop similar delays.

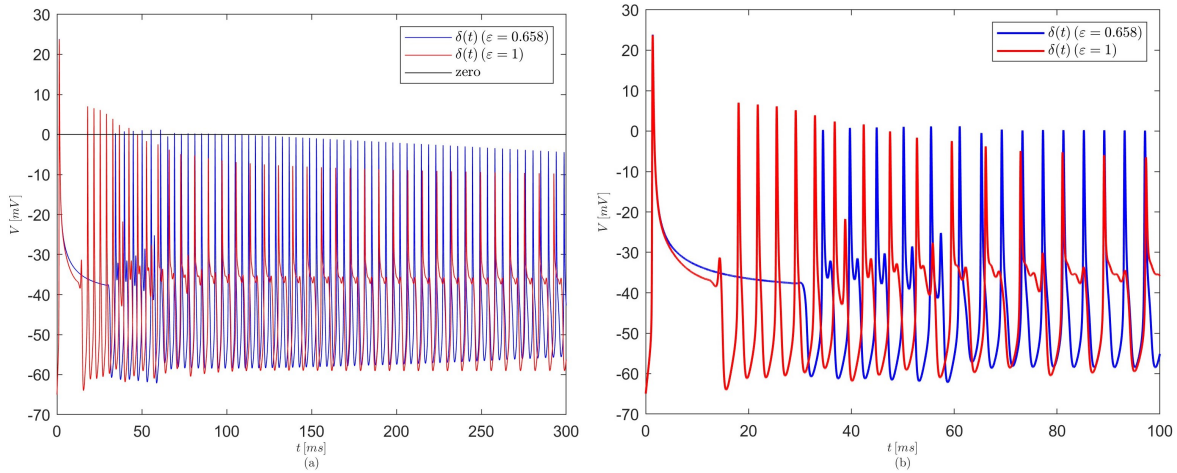

Figure 15. (**a**) Comparison of action potentials for viscoelastic memory $\delta(t)$ given by Formula (30) with $\delta_{AD} = 0.5$ and with Fickian ($\varepsilon = 1$) and non-Fickian ($\varepsilon = 0.658$) release of donepezil. (**b**) Zoomed-in view of the plots in (**a**). Plots not to scale. The action potentials after donepezil intake with Fickian release have positive overshoots and reach the normal resting potential for a short time. The first plateau region is shorter than the one corresponding to the action potentials after donepezil treatment with non-Fickian release and develop short plateau regions at later times. On the other hand, the action potentials after donepezil intake with non-Fickian drug release do not have positive overshoots, have a longer first plateau region, followed by a few shorter plateau regions, and oscillations with no delays at later times.

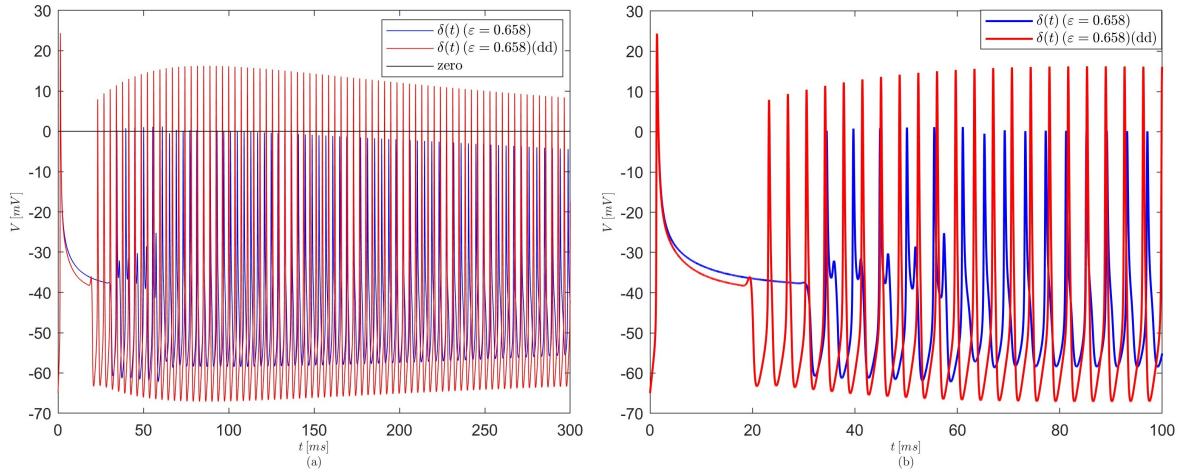

Figure 16. (**a**) Comparison of action potentials for viscoelastic memory $\delta(t)$ given by Formula (30) with $\delta_{AD} = 0.5$, non-Fickian ($\varepsilon = 0.658$) release of donepezil, and with either single (250 μg; blue line) or double (500 μg; red line) dose of orally administered donepezil. (**b**) Zoomed-in view of the plots in (**a**). In the legend maps, (dd) stands for double dose. Plots not to scale. The potential corresponding to the double dose has a shorter initial delay, reaches the normal rest potential and higher amplitudes of positive overshoots that slowly decay at later times.

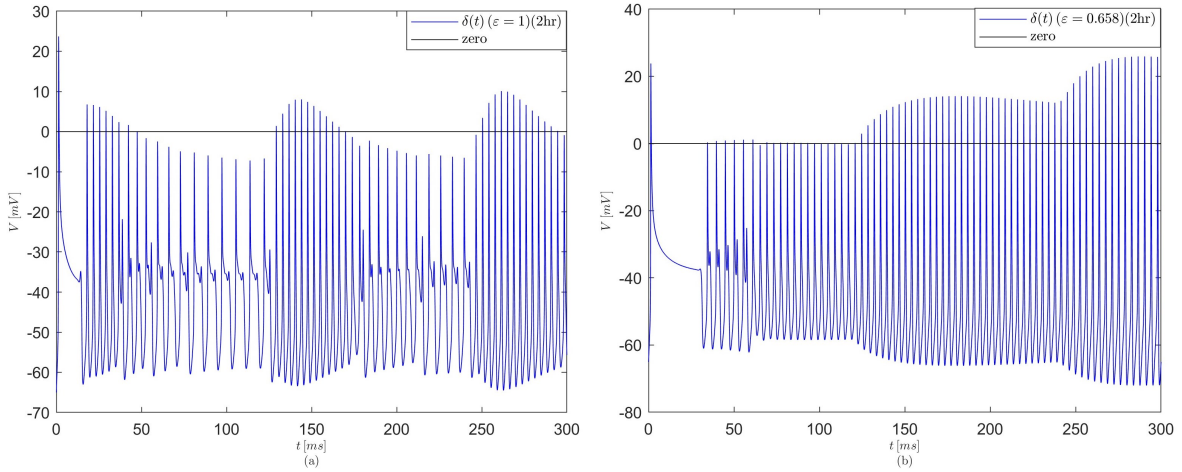

Figure 17. Action potentials for viscoelastic memory $\delta(t)$ given by Formula (30) with $\delta_{AD} = 0.5$ and with (**a**) Fickian ($\varepsilon = 1$) and (**b**) non-Fickian ($\varepsilon = 0.658$) release of donepezil. The administered dosage is 250 μg every 120 min during the observed period of 600 min. In the legend maps, (2 h) stands for the administration of donepezil every two hours. Plots not to scale. The action potentials corresponding to $\varepsilon = 1$ start sooner, the amplitudes of the positive overshoots slowly increase with each administration of donepezil, and there are regions with no positive overshoots which have smaller frequencies and small delays. The action potentials corresponding to $\varepsilon = 0.658$ start later, the amplitudes of the positive overshoots increase with each administration of donepezil, and there are no regions that lack positive overshoots.

If $\delta_{AD} = 0.75$, the intake of donepezil recovers the ability of the membrane potential to have positive overshoots and reach the resting membrane potential V_{rest} in Table 1 for a longer time (about 600 min, see Figure 10c) and both the amplitude and peak-to-peak amplitude of the oscillations are larger when the controlled release uses $\varepsilon = 0.658$ instead of $\varepsilon = 1$ (Figure 13). On the other hand, if $\delta_{AD} = 0.5$ the action potentials reach the resting potential V_{rest} and have positive overshoots for a shorter time (about 100 min, see Figure 10c) if the administered donepezil is released with $\varepsilon = 1$. The action potentials for

$\delta(t) = 0.5 + c_{\text{brain}}$ do not change significantly from those corresponding to $\delta_{AD} = 0.5$ when a controlled release donepezil with $\varepsilon = 0.658$ is administered (Figure 15).

For later stages of AD described by $\delta_{AD} = 0.5$, an increase in donepezil dosage (quantity and/or frequency) is needed to get shorter viscoelastic memory (see Figure 11) and corresponding improved action potentials. Figure 16 shows action potentials for $\delta_{AD} = 0.5$, $\varepsilon = 0.658$ when a double dose of donepezil (500 μg) is administered initially. The potential experiences a shorter initial delay than the case when the administered drug dose is 250 μg, reaches the rest potential and higher amplitudes of positive overshoots that slowly decay at later times in a manner similar to the associated $\delta(t)$ (Figure 11). If $\delta_{AD} = 0.5$ and the drug dose of 250 μg is administered every two hours then the action potentials corresponding to $\varepsilon = 1$ start sooner and although the amplitudes of the positive overshoots slowly increase with each administration of donepezil there are still regions with no positive overshoots, smaller frequencies and small delays (Figure 17a). If $\varepsilon = 0.658$, the positive overshoots are delayed, and their amplitudes increase with each administration of donepezil. Also, in this case, the positive overshoots are not interrupted by regions lacking positive overshoots (Figure 17b). These observations suggest that combining various donepezil's release modalities and dosages may provide better treatments for AD than treatments that use the same release approach with different donepezil dosages for all stages of AD.

Lastly, the convergence of the numerical scheme used to solve system (20)–(23) for a variable fractional order $\delta(t)$ was studied for the case $\delta_{AD} = 0.75$, $\varepsilon = 0.658$, and the time step sizes $\Delta t_1 = 0.005$, $\Delta t_{1/2} = \Delta t_1/2$, and $\Delta t_{1/4} = \Delta t_1/4$. Let $V(\Delta t_i)$ denote the numerical solution of Equation (20) for the step size Δt_i and $i \in \{1, 1/2, 1/4\}$. Then the following relative errors were calculated [88]:

$$E_1 = \frac{\|V(\Delta t_1) - V(\Delta t_{1/4})\|_{L^2(\mathbb{R})}}{\|V(\Delta t_{1/4})\|_{L^2(\mathbb{R})}}, E_{1/2} = \frac{\|V(\Delta t_{1/2}) - V(\Delta t_{1/4})\|_{L^2(\mathbb{R})}}{\|V(\Delta t_{1/4})\|_{L^2(\mathbb{R})}}.$$

The order of convergence was also calculated as:

$$p = \log_2\left(\frac{\|V(\Delta t_1) - V(\Delta t_{1/2})\|_{L^2(\mathbb{R})}}{\|V(\Delta t_{1/2}) - V(\Delta t_{1/4})\|_{L^2(\mathbb{R})}}\right).$$

The results of these calculations are shown in Table 3. The convergence is linear since $p \approx 1$.

Table 3. Relative errors and order of convergence for the numerical scheme used to solve the generalized Hodgkin-Huxley equations with a variable fractional order $\delta(t)$.

E_1	$E_{1/2}$	p
0.3557	0.1474	0.8662(≈1)

5. Discussion and Conclusion Remarks

In this paper, mathematical modeling is used to study the transport to the brain of anomalous release donepezil and the effect of donepezil on action potentials. Caputo fractional derivatives are used to model anomalous release patterns of donepezil and the viscoelastic behavior of ligand-gated ion channels. A generalized pharmacokinetic model for the transport to the brain of anomalous release donepezil is proposed and its analytic and numeric solutions are found and shown to be in perfect agreement. A generalized Hodgkin-Huxley model is also proposed that couples the electric activity of neuronal membrane and the viscoelastic behavior of the ion channels. The variable-order fractional Maxwell linear viscoelastic model is used to describe the viscoelasticity of ion channels. The variable-order Caputo fractional derivative is chosen to model viscoelastic fading memory since it has no memory of its past order and thus it can transfer to the output

specific features (such as monotonicity or oscillatory behavior) of the fractional variable order. The Haar piecewise-constant approximants of specific variable fractional orders were used, in combination with properties of constant-order Caputo fractional derivatives, to characterize the corresponding creep and relaxation responses of the chosen viscoelastic model. The action potentials predicted by the generalized Hodgkin-Huxley model depend on the viscoelastic fading memory of the ion channels as follows. For shorter fading memory (fractional order closer to 1), the action potentials have shapes similar to those predicted by the classic Hodgkin-Huxley model and thus they are considered to be generated by a functional neuron with structurally intact ion channels. For longer fading memory (fractional order closer to 0), abnormal patterns of action potentials are obtained that correspond to dysfunctional neurons with structurally damaged ion channels. Based on a qualitative visual matching of the shapes of abnormal action potentials predicted by the proposed model and the shapes of action potentials in the presence of AD available in the literature, two constant values of the fractional order are chosen to correspond to earlier ($\delta_{AD} = 0.75$) and later ($\delta_{AD} = 0.5$) stages of AD. The coupling of the generalized pharmacokinetic and Hodgkin-Huxley models is based on the following assumptions: the concentration of donepezil is proportional to the concentration of ACh made available by donepezil intake, and the temporary binding between ACh and its ligand-gated ion channels confers the shorter viscoelastic fading memory to the channels needed to generate healthy action potentials. By taking the variable fractional order describing the viscoelastic memory of ion channels to be the addition of the δ_{AD} and a rescaled and dimensionless concentration of donepezil in the brain, the effects of donepezil intake on the action potentials can be observed. The lack of past order memory of the chosen variable-order fractional derivative allows for the transfer to the action potentials of the temporal variations of the amount of ACh. The results show that: (1) in the brain, an anomalous release donepezil decays slower than a donepezil solution available on the market, (2) donepezil intake temporarily recovers healthy action potentials which agrees with clinical observations [7], and (3) for later stages of AD, combinations of various release modalities and dosages of donepezil may provide better treatment outcomes.

Neuronal structural damage and dysfunction are pathological hallmarks of neurodegenerative disorders. Although these disorders have specific biochemical pathways of progression, they share certain patterns of structural and functional abnormalities. For instance, AD animal models showed that the accumulation of $A\beta$ plaques and NFT can cause myelin damage and oligodendrocyte deterioration leading to demyelienation that further contributes to the progression of AD. The AD-associated demyelienation happens years before the first symptoms of AD emerge and has neuroimaging presentations similar to the demyelienation seen in multiple sclerosis [10–13]. AD and stroke are also interrelated disorders [89]. Strokes cause, among others, an impaired cerebral blood flow, neural injury and depolarization, neuroinflammation, and damage to the blood-brain barrier, which could result in AD onset and progression years later. On the other hand, AD causes the disintegration of the blood-brain barrier that further leads to impaired diffusion and interstitial fluid flow within the cerebral extracellular space, enhanced cerebral inflammatory and immune responses, progression of AD, and, potentially, strokes [4,90,91]. Structural damage of ion channels were also associated with AD and other neurodegenerative disorders [15,47,48,82].

The abnormal patterns of action potentials in the presence of AD predicted by the proposed generalized Hodgkin-Huxley model are similar to those seen in untreated AD and other neurodegenerative disorders. Various studies have shown hyperexcitability and epileptiform activity in early stages of AD, followed by increasing lack of action potentials in later stages of AD [9,14,15,17,44,45]. Figure 7 shows that, as δ decreases from 1, the current activation happens at less negative voltages (higher resting potential), inactivation occurs at less positive voltages (smaller positive overshoots), and the action potentials experience decreasing amplitudes and smaller frequencies, which, by definition, correspond to a loss of function phenotype introduced in [15]. The case $\delta_{AD} = 0.75$ shows plateau (delayed) potentials followed by higher frequency of firing which correspond to hyperexcitability seen

in earlier stages of AD. Similar patterns of action potentials were observed experimentally in transgenic Na v1.8-null knockout DRG neurons [92], abnormal Na v1.8 expression in some neurons that may be linked to multiple sclerosis [93], and mutations of some sodium channels that cause persistent sodium currents linked to epilepsy [94,95]. The case $\delta_{AD} = 0.5$ (and lower values of δ) shows an almost cessation of action potentials that may be associated with later stages of AD [17]. Similar abnormal action potentials were observed experimentally in neurons under spreading depolarization (that may happen in ischemic stroke) and a blockade of astrocytic glutamate transporters [96]. The abnormal action potentials also look similar to some of the membrane voltages predicted by the mathematical models proposed in [44,45,97,98]. The models in [44,45] were obtained by coupling the Hodgkin-Huxley model and ion concentration dynamics observed in AD animal models via the Nernst equations. The models in [97,98] are not specific to AD and are obtained by mathematical modifications of the Hodgkin-Huxley model. While a combination of Taylor's formula for multivariable functions and various external stimuli is used in [97], the concept of a two-terminal resistor with memory called memristor is introduced in [98] and the so-called memristive Hodgkin-Huxley model is then obtained by replacing the sodium and potassium conductances in the classic Hodgkin-Huxley model by flux-controlled memristors. A major difference between the proposed generalized Hodgkin-Huxley model and published mathematical models is the level of complexity. Models existing in the literature have a high level of complexity; they use many variables and parameters to predict abnormal action potentials. On the other hand, only the memory parameter of the generalized Hodgkin-Huxley model needs to be modified to predict healthy and various abnormal patterns of action potentials. Neither the recovery of the healthy patterns of action potentials after the administration of AD therapies nor the transport of anomalous release donepezil to the brain have been reported in the literature until now.

Lastly, the proposed generalized Hodgkin-Huxley and coupled models require experimental validation. For the calibration of the models, it is important to find the values of the moduli of elasticity, generalized viscosities, and memory parameters of the nicotinic ACh receptors (and neuronal ion channels in general) in properly functioning neurons and in neurons altered by the AD progression, as well as their dependencies on electric currents and, in the case of AD, the concentration of orally administered donepezil in the brain. Currently, there are no published viscoelastic characterizations of neuronal ion channels. However, optical tweezers-based microrheology [99–101] and optical coherence elastography [102] are non-invasive and contactless techniques that can be used in vivo and in vitro to study mechanical properties of biological structures at (sub)micron levels like ion channels. In optical tweezers-based microrheology, small particles are trapped and manipulated using a highly focused laser beam and measurements of the light scattered by the trapped particles moving through a material provide the viscoelastic properties of the material. Of particular interest to the work in this paper could be the active–passive calibration technique proposed in [101] that can measure viscoelastic properties of a material over a wide frequency range with high spatio-temporal resolution. In optical coherence elastography, the deformation in a material subjected to a mechanical force is measured using optical coherence tomography, and then an inverse problem is solved with the known deformation to find the viscoelastic properties of the material. Initially, these two technologies could be used with animal models of AD to find the viscoelastic properties of retinal neurons.

Future work will explore the generalized Hodgkin-Huxley model for distinct memory parameters of the ion channels, in the presence of various external stimuli and ion concentration dynamics. The derivation of semi-analytic solutions to the generalized Hodgkin-Huxley model using Haar wavelets will also be investigated.

Funding: This research received no external funding.

Data Availability Statement: The original contributions presented in the study are included in the article, further inquiries can be directed to the corresponding author.

Conflicts of Interest: The author declares no conflicts of interest. The funders had no role in the design of the study; in the collection, analyses, or interpretation of data; in the writing of the manuscript; or in the decision to publish the results.

Abbreviations

The following abbreviations are used in this manuscript:

AD	Alzheimer's disease
$A\beta$	Amyloid-β
NFT	Neurofibrillary tangles
AChE	Acetylcholinesterase
ACh	Acetylcholine

Appendix A

The descriptions and physical units of the variables of the models presented in Sections 3.2 and 3.3 are given in Table A1.

Table A1. The values, physical units, and descriptions of the models' variables.

Variables	Physical Units	Description
t	ms (Section 3.2), min (Section 3.3)	time
V	mV	Membrane potential
m		Nondimensional displacement of the activating sodium gate
h		Nondimensional displacement of the inactivating sodium gate
n		Nondimensional displacement of the activating potassium gate
c_d	$\mu g/mL$	Donepezil concentration in the depot
c_{blood}	$\mu g/mL$	Donepezil concentration in the blood
c_{brain}	$\mu g/mL$	Donepezil concentration in the brain
c_p	$\mu g/mL$	Donepezil concentration in the periphery

References

1. Alzheimer, A. Uber einen eigenartigen schweren Erkrankungsprozess der Hirninde. *Neurol. Centralblatt.* **1906**, *25*, 1134.
2. World Health Organization. Dementia Key Facts. Available online: https://www.who.int/news-room/fact-sheets/detail/dementia (accessed on 20 July 2024).
3. Carreiras, M.C.; Mendes, E.; Perry, M.J.; Francisco, A.P.; Marco-Contelles, J. The multifactorial nature of Alzheimer's disease for developing potential therapeutics. *Curr. Top. Med. Chem.* **2013**, *13*, 1745–1770. [CrossRef] [PubMed]
4. Sweeney, M.D.; Sagare, A.P.; Zlokovic, B.V. Blood–brain barrier breakdown in Alzheimer disease and other neurodegenerative disorders. *Nat. Rev. Neurol.* **2018**, *14*, 133–150. [CrossRef] [PubMed]
5. Salman, M.M.; Kitchen, P.; Halsey, A.; Wang, M.X.; Törnroth-Horsefield, S.; Conner, A.C.; Badaut, J.; Iliff, J.J.; Bill, R.M. Emerging roles for dynamic aquaporin-4 subcellular relocalization in CNS water homeostasis. *Brain* **2022**, *145*, 64–75. [CrossRef]
6. Kinney, J.W.; Bemiller, S.M.; Murtishaw, A.S.; Leisgang, A.M.; Salazar, A.M.; Lamb, B.T. Inflammation as a central mechanism in Alzheimer's disease. *Alzheimer's Dement. Transl. Res. Clin. Interv.* **2018**, *4*, 575–590. [CrossRef]
7. Marucci, G.; Buccioni, M.; Dal Ben, D.; Lambertucci, C.; Volpini, R.; Amenta, F. Efficacy of acetylcholinesterase inhibitors in Alzheimer's disease. *Neuropharmacology* **2021**, *190*, 108352. [CrossRef]
8. Garcia-Ayllon, M.-S.; Small, D.H.; Avila, J.; Saez-Valero, J. Revisiting the role of acetylcholinesterase in Alzheimer's disease: Cross-talk with P-tau and β-amyloid. *Front. Mol. Neurosci.* **2011**, *4*, 22. [CrossRef]
9. Anastacio, H.T.D.; Matosin, N.; Ooi, L. Neuronal hyperexcitability in Alzheimer's disease. what are the drivers behind this aberrant phenotype? *Transl. Psychiatry* **2022**, *12*, 257. [CrossRef]
10. Nasrabady, S.E.; Rizvi, B.; Goldman, J.E.; Brickman, A.M. White matter changes in Alzheimer's disease: A focus on myelin and oligodendrocytes. *Acta Neuropathol. Commun.* **2018**, *6*, 22. [CrossRef]
11. Depp, C.; Sun, T.; Sasmita, A.O.; Spieth, L.; Berghoff, S.A.; Nazarenko, T.; Overhoff, K.; Steixner-Kumar, A.A.; Subramanian, S.; Arinrad, S.; et al. Myelin dysfunction drives amyloid-β deposition in models of Alzheimer's disease. *Nature* **2023**, *618*, 349–357. [CrossRef]

12. Dan, L.; Zhang, Z. Alzheimer's disease: An axonal injury disease? *Front. Aging Neurosci.* **2023**, *15*, 1264448. [CrossRef] [PubMed]
13. Boukhvalova, M.S.; Kastrukoff, L.; Blanco, J.C.G. Alzheimer's disease and multiple sclerosis: A possible connection through the viral demyelinating neurodegenerative trigger (vDENT). *Front. Aging Neurosci.* **2023**, *15*, 1204852. [CrossRef] [PubMed]
14. Yavorsky, V.A.; Rozumna, N.M.; Lukyanetz, E.A. Influence of amyloid beta on impulse spiking of isolated hippocampal neurons. *Front. Cell. Neurosci.* **2023**, *17*, 1132092. [CrossRef] [PubMed]
15. Barbieri, R.; Nizzari, M.; Zanardi, I.; Pusch, M.; Gavazzo, P. Voltage-gated sodium channel dysfunctions in neurological disorders. *Life* **2023**, *13*, 1191. [CrossRef]
16. Melgosa-Ecenarro, L.; Doostdar, N.; Radulescu, C.I.; Jackson, J.S.; Barnes, S.J. Pinpointing the locus of GABAergic vulnerability in Alzheimer's disease. *Semin. Cell Dev. Biol.* **2023**, *139*, 35–54. [CrossRef]
17. Tzavellas, N.P.; Tsamis, K.I.; Katsenos, A.P.; Davri, A.S.; Simos, Y.V.; Nikas, I.P.; Bellos, S.; Lekkas, P.; Kanellos, F.S.; Konitsiotis, S.; et al. Firing alterations of neurons in Alzheimer's disease: Are they merely a consequence of pathogenesis or a pivotal component of disease progression? *Cells* **2024**, *13*, 434. [CrossRef]
18. Kumar, A.; Gupta, V.; Sharma, S. Donepezil. In *StatPearls*; StatPearls Publishing: Treasure Island, FL, USA, 2024. Available online: https://www.ncbi.nlm.nih.gov/books/NBK513257/ (accessed on 20 July 2024).
19. Sam, C.; Bordoni, B. Physiology, Acetylcholine. In *StatPearls*; StatPearls Publishing: Treasure Island, FL, USA, 2024. Available online: https://www.ncbi.nlm.nih.gov/books/NBK557825/ (accessed on 16 August 2024).
20. Carlson, A.B.; Kraus, G.P. Physiology, Cholinergic Receptors. In *StatPearls*; StatPearls Publishing: Treasure Island, FL, USA, 2024. Available online: https://www.ncbi.nlm.nih.gov/books/NBK526134/ (accessed on 8 December 2024).
21. Kim, J.; Lee, H.J.; Park, S.K.; Park, J.H.; Jeong, H.R.; Lee, S.; Lee, H.; Seol, E.; Hoe, H.S. Donepezil regulates LPS and $A\beta$-stimulated neuroinflammation through MAPK/NLRP3 inflammasome/STAT3 signaling. *Int. J. Mol. Sci.* **2021**, *22*, 10637. [CrossRef]
22. Lombardo, S.; Maskos, U. Role of the nicotinic acetylcholine receptor in Alzheimer's disease pathology and treatment. *Neuropharmacology* **2015**, *96 Pt B*, 255–262. [CrossRef]
23. Monaco, M.; Trebesova, H.; Grilli, M. Muscarinic receptors and Alzheimer's disease: New perspectives and mechanisms. *Curr. Issues Mol. Biol.* **2024**, *46*, 6820–6835. [CrossRef]
24. Jakki, S.L.; Ramesh, Y.V.; Gowthamarajan, K.; Senthil, V.; Jain, K.; Sood, S.; Pathak, D. Novel anionic polymer as a carrier for CNS delivery of anti-Alzheimer drug. *Drug Deliv.* **2016**, *23*, 3471–3479. [CrossRef]
25. Silva, R.O.; Counil, H.; Rabanel, J.-M.; Haddad, M.; Zaouter, C.; Khedher, M.R.B.; Patten, S.A.; Ramassamy, C. Donepezil-loaded nanocarriers for the treatment of Alzheimer's disease: Superior efficacy of extracellular vesicles over polymeric nanoparticles. *Int. J. Nanomed.* **2024**, *19*, 1077–1096. [CrossRef] [PubMed]
26. Topal, G.R.; Mészáros, M.; Porkoláb, G.; Szecskó, A.; Polgár, T.F.; Siklós, L.; Deli, M.A.; Veszelka, S.; Bozkir, A. ApoE-targeting increases the transfer of solid lipid nanoparticles with donepezil cargo across a culture model of the blood–brain barrier. *Pharmaceutics* **2021**, *13*, 38. [CrossRef] [PubMed]
27. Topal, G.R.; Kücüktürkmen, B.; Öz, U.C.; Özkan, E.; Bakar-Ates, F.; Bozkir, A. Investigation on formulation parameters of donepezil HCl loaded solid lipid nanoparticles. *Braz. J. Pharm. Sci.* **2023**, *59*, e22330. [CrossRef]
28. Tao, X.; Mao, S.; Zhang, Q.; Yu, H.; Li, Y.; He, X.; Yang, S.; Zhang, Z.; Yi, Z.; Song, Y.; et al. Brain-targeted polysorbate 80-emulsified donepezil drug-loaded nanoparticles for neuroprotection. *Nanoscale Res. Lett.* **2021**, *16*, 132. [CrossRef]
29. Akyol, E.; Senol, S.; Dogan, Ö. Controlled release of donepezil hydrochloride from the ternary sodium alginate based hydrogels. *Bulg. Chem. Commun.* **2017**, *49*, 57–63.
30. Ruela, A.L.; Carvalho, F.C.; Pereira, G.R. Exploring the phase behavior of monoolein/oleic acid/water Systems for enhanced donezepil administration for Alzheimer disease treatment. *J. Pharm. Sci.* **2016**, *105*, 71–77. [CrossRef]
31. Bulut, E.; Sanli, O. Delivery of Alzheimer's drug donepezil hydrochloride from ionically crosslinked alginate microspheres prepared by water-in-oil emulsion technique: Optimization of release conditions. *Asian J. Chem.* **2013**, *25*, 3993–4000. [CrossRef]
32. Kaikousidis, C.; Papakyriakopoulou, P.; Dokoumetzidis, A.; Valsami, G. Donepezil brain and blood pharmacokinetic modeling after nasal film and oral solution administration in mice. *Pharmaceutics* **2023**, *15*, 1409. [CrossRef]
33. Papakyriakopoulou, P.; Balafas, E.; Colombo, G.; Rekkas, D.M.; Kostomitsopoulos, N.; Valsami, G. Nose-to-brain delivery of donepezil hydrochloride following administration of an HPMC-Me-β-CD-PEG400 nasal film in mice. *J. Drug Deliv. Sci. Technol.* **2023**, *84*, 104463. [CrossRef]
34. Espinoza, L.C.; Guaya, D.; Calpena, A.C.; Perotti, R.M.; Halbaut, L.; Sosa, L.; Brito-Llera, A.; Mallandrich, M. Comparative study of donepezil-loaded formulations for the treatment of Alzheimer's disease by nasal administration. *Gels* **2022**, *8*, 715. [CrossRef]
35. Zhang, P.; Chen, L.; Gu, W.; Xu, Z.; Gao, Y.; Li, Y. In vitro and in vivo evaluation of donepezil-sustained release microparticles for the treatment of Alzheimer's disease. *Biomaterials* **2007**, *28*, 1882–1888. [CrossRef] [PubMed]
36. Kearney, M.-C.; Caffarel-Salvador, E.; Fallows, S.J.; McCarthy, H.O.; Donnelly, R.F. Microneedle-mediated delivery of donepezil: Potential for improved treatment options in Alzheimer's disease. *Eur. J. Pharm. Biopharm.* **2016**, *103*, 43–50. [CrossRef] [PubMed]
37. Bruschi, M.L. *Strategies to Modify the Drug Release from Pharmaceutical Systems*; Woodhead Publishing: Cambridge, UK, 2015; pp. 63–86.
38. Trucillo, P. Drug carriers: A review on the most used mathematical models for drug release. *Processes* **2022**, *10*, 1094. [CrossRef]
39. Khanday, M.A.; Rafiq, A.; Nazir, K. Mathematical models for drug diffusion through the compartments of blood and tissue medium. *Alex. J. Med.* **2017**, *53*, 245–249. [CrossRef]

40. Shyamsunder, S.; Bhatter, K.J.; Purohit, S.D. Fractionalized mathematical models for drug diffusion. *Chaos Solitons Fractals* **2022**, *165*, 112810. [CrossRef]
41. Alijani, Z.; Shiri, B.; Perfilieva, I.; Baleanu, D. Numerical solution of a new mathematical model for intravenous drug administration. *Evol. Intel.* **2024**, *17*, 559–575. [CrossRef]
42. Hodgkin, A.L.; Huxley, A.F. A quantitative description of membrane current and its application to conduction and excitation in nerve. *J. Physiol.* **1952**, *117*, 500–544. [CrossRef]
43. Wei, Y.; Ullah, G.; Schiff, S.J. Unification of neuronal spikes, seizures, and spreading depression. *J. Neurosci.* **2014**, *34*, 11733–11743. [CrossRef]
44. Perez, C.; Ziburkus, J.; Ullah, G. Analyzing and modeling the dysfunction of inhibitory neurons in Alzheimer's disease. *PLoS ONE* **2016**, *11*, e0168800. [CrossRef]
45. Adeoye, T.; Shah, S.I.; Demuro, A.; Rabson, D.A.; Ullah, G. Upregulated Ca^{2+} release from the endoplasmic reticulum leads to impaired presynaptic function in familial Alzheimer's disease. *Cells* **2022**, *11*, 2167. [CrossRef]
46. Gupta, S.; Singh, J.; Kumar, K. Ionic concentration and action potential differences between a healthy and Alzheimer's disease person. In Proceedings of the 5th International Conference on Recent Developments in Science, Engineering and Technology (REDSET 2019), Gurugram, India, 15–16 November 2019; Batra, U., Roy, N., Panda, B., Eds.; Communications in Computer and Information Science; Springer Nature: Cham, Switzerland, 2020; Volume 1229, pp. 266–277.
47. Purves, D.; Augustine, G.J.; Fitzpatrick, D.; Katz, L.C.; LaMantia, A.-S.; McNamara, J.O.; Williams, S.M. Cholinergic Receptors. In *Neuroscience*, 2nd ed.; Sinauer Associates: Sunderland, MA, USA, 2001.
48. Zoli, M.; Pucci, S.; Vilella, A.; Gotti, C. Neuronal and extraneuronal nicotinic acetylcholine receptors. *Curr. Neuropharmacol.* **2018**, *16*, 338–349. [PubMed]
49. Metzler, R.; Klafter, J. The restaurant at the end of the random walk: Recent developments in the description of anomalous transport by fractional dynamics. *J. Phys. A Math. Gen.* **2004**, *37*, R161.
50. Mainardi, F. *Fractional Calculus and Waves in Linear Viscoelasticity*; Imperial College Press: London, UK, 2010.
51. Drapaca, C.S. Fractional calculus in neuronal electromechanics. *J. Mech. Mater. Struct.* **2017**, *12*, 35–55. [CrossRef]
52. Drapaca, C.S. A nitric oxide-modulated variable-order fractional Maxwell viscoelastic model of cerebral vascular walls. *Front. Mech. Eng* **2021**, *7*, 674860.
53. Samko, S.; Kilbas, A.A.; Marichev, O.I. *Fractional Integrals and Derivatives: Theory and Applications*; Gordon and Breach Science Publishers: London, UK, 2000.
54. Gorenflo, R.; Mainardi, F. Fractional calculus: Integral and differential equations of fractional order. In *Fractals and Fractional Calculus in Continuum Mechanics*; Carpinteri, A., Mainardi, F., Eds.; Springer: Wien, Austria; New York, NY, USA, 1997; pp. 223–276.
55. Sambandham, B.; Vatsala, A.S. Basic results for sequential Caputo fractional differential equations. *Mathematics* **2015**, *3*, 76–91. [CrossRef]
56. Sun, H.G.; Chang, A.; Zhang, Y.; Chen, W. A review on variable-order fractional differential equations: Mathematical foundations, physical models, numerical methods and applications. *Fract. Calc. Appl. Anal.* **2019**, *22*, 27–59.
57. Patnaik, S.; Hollkamp, J.P.; Semperlotti, F. Applications of variable-order fractional operators: A review. *Proc. R. Soc. A* **2020**, *476*, 20190498.
58. Moghaddam, B.P.; Machado, J.A.T. Extended algorithms for approximating variable order fractional derivatives with applications. *J. Sci. Comput.* **2017**, *71*, 1351–1374.
59. Baleanu, D.; Diethelm, K.; Scalas, E.; Trujillo, J.J. *Fractional Calculus Models and Numerical Methods*; World Scientific: Hackensack, NJ, USA, 2012.
60. Atangana , A.; Secer, A. A note on fractional order derivatives and table of fractional derivatives of some special functions. *Abstr. Appl. Anal.* **2013**, *2013*, 279681.
61. Haar, A. Zur Theories der orthogonalen Funktionensystem. *Math. Annal.* **1910**, *69*, 331–371. [CrossRef]
62. Volker, M. *Lectures on Constructive Approximation: Fourier, Spline, and Wavelet Methods on the Real Line, the Sphere, and the Ball*; Birkhauser: Boston, MA, USA, 2013.
63. Addison, P.S. *The Illustrated Wavelet Transform Handbook Introductory Theory and Applications in Science, Engineering, Medicine and Finance*, 2nd ed.; CRC Press: Boca Raton, FL, USA, 2020.
64. Chen, C.F.; Hsiao, C.H. Haar wavelet method for solving lumped and distributed-parameter system. *IEEE Proc. Control Theory Appl.* **1997**, *144*, 87–94. [CrossRef]
65. Lepik, U. Numerical solution of differential equations using Haar wavelets. *Math. Comput. Simul.* **2005**, *68*, 127–143. [CrossRef]
66. Lepik, U. Solving differential and integral equations by the Haar wavelet method; revisited. *Int. J. Math. Comput.* **2008**, *1*, 43–52.
67. Aziz, I.; Amin, R. Numerical solution of a class of delay differential and delay partial differential equations via Haar wavelet. *Appl. Math. Model.* **2016**, *40*, 10286–10299. [CrossRef]
68. Gupta, A.K.; Ray, S.S. Wavelet methods for solving fractional order differential equations. *Math. Probl. Eng.* **2014**, *2014*, 140453. [CrossRef]
69. Heil, C. *A Basis Theory Primer: Expanded Edition (Applied and Numerical Harmonic Analysis)*; Birkhauser: Boston, MA, USA, 2010.
70. The MathWorks Inc. *MATLAB*, version 24.1.0.2537033 (R2024a); The MathWorks Inc.: Natick, MA, USA, 2024.
71. Ramirez, L.; Coimbra, C. On the selection and meaning of variable order operators for dynamic modeling. *Int. J. Diff. Equ.* **2010**, *2010*, 846107. [CrossRef]

72. Lorenzo, C.F.; Hartley, T.T. Variable order and distributed order fractional operators. *Nonlinear Dyn.* **2002**, *29*, 57–98. [CrossRef]
73. Sun, H.; Chen, W.; Wei, H.; Chen, Y. A comparative study of constant-order and variable-order fractional models in characterizing memory property of systems. *Eur. Phys. J. Spec. Top.* **2011**, *193*, 185–192. [CrossRef]
74. Bazhlekova, E.; Bazhlekov, I. Stokes' first problem for viscoelastic fluids with a fractional Maxwell model. *Fractal Fract.* **2017**, *1*, 7. [CrossRef]
75. Findley, W.N.; Lai, J.S.; Onaran, K. *Creep and Relaxation of Nonlinear Viscoelastic Materials—With an Introduction to Linear Viscoelasticity*; Dover Publications: Garden City, NY, USA, 1989.
76. Pipkin, A.; Rogers, T. A non-linear integral representation for viscoelastic behavior. *J. Mech. Phys. Solids* **1968**, *16*, 59–72. [CrossRef]
77. Fréchet, M. Sur les fonctionnelles continues. *Ann. De L'Ecole Norm.* **1910**, *3*, 193–216. [CrossRef]
78. Volterra, V. *Theory of Functionals and the Integral and Integro-Differential Equations*; Dover Publications: Garden City, NY, USA, 1959.
79. Bonilla, B.; Rivero, M.; Trujillo, J.J. On systems of linear fractional differential equations with constant coefficients. *Appl. Math. Comput.* **2007**, *187*, 68–78. [CrossRef]
80. Odibat, Z.M. Analytic study on linear systems of fractional differential equations. *Comput. Math. Appl.* **2010**, *59*, 1171–1183. [CrossRef]
81. Wineman, A.S.; Rajagopal, K.R. *Mechanical Response of Polymers: An Introduction*, 1st ed.; Cambridge University Press: Cambridge, UK, 2000.
82. Lehmann-Horn, F.; Jurkat-Rott, K. Voltage-gated ion channels and hereditary disease. *Physiol. Rev.* **1999**, *79*, 1317–1372. [CrossRef] [PubMed]
83. Gautieri, A.; Vesentini, S.; Redaelli, A.; Buehler, M.J. Viscoelastic properties of model segments of collagen molecules. *Matrix Biol.* **2012**, *31*, 141–149. [CrossRef] [PubMed]
84. Hayek, N.; Trujillo, J.J.; Rivero, M.; Bonilla, B.; Moreno, J.C. An extension of Picard–Lindeloff theorem to fractional differential equations. *Appl. Anal.* **1999**, *70*, 347–361. [CrossRef]
85. Almeida, R.; Malinowska, A.B.; Odzijewicz, T. On systems of fractional differential equations with the ψ-Caputo derivative and their applications. *Math. Meth. Appl. Sci.* **2021**, *44*, 8026–8041. [CrossRef]
86. Shampine, L.F.; Reichelt, M.W. The MATLAB ODE suite. *SIAM J. Sci. Comput.* **1997**, *18*, 1–22. [CrossRef]
87. Garrappa, R. Numerical solution of fractional differential equations: A survey and a software tutorial. *Mathematics* **2018**, *6*, 16. [CrossRef]
88. LeVeque, R.J. *Finite Difference Methods for Ordinary and Partial Differential Equations: Steady-State and Time-Dependent Problems*, 1st ed.; Society for Industrial and Applied Mathematics: Philadelphia, PA, USA, 2007; pp. 254–258.
89. Gupta, A.; Uthayaseelan, K.; Uthayaseelan, K.; Kadari, M.; Subhan, M.; Saji Parel, N.; Krishna, P.V.; Sange, I. Alzheimer's disease and stroke: A tangled neurological conundrum. *Cureus* **2022**, *14*, e25005. [CrossRef]
90. Montagne, A.; Zhen Zhao, Z.; Zlokovic, B.V. Alzheimer's disease: A matter of blood–brain barrier dysfunction? *J. Exp. Med.* **2017**, *214*, 3151–3169. [CrossRef] [PubMed]
91. Alkhalifa, A.E.; Al-Ghraiybah, N.F.; Odum, J.; Shunnarah, J.G.; Austin, N.; Kaddoumi, A. Blood–brain barrier breakdown in Alzheimer's disease: Mechanisms and targeted strategies. *Int. J. Mol. Sci.* **2023**, *24*, 16288. [CrossRef] [PubMed]
92. Renganathan, M.; Cummins, T.R.; Waxman, S.G. Contribution of Nav 1.8 sodium channels to action potential electrogenesis in DRG neurons. *J. Neurophysiol.* **2001**, *86*, 629–640. [CrossRef] [PubMed]
93. Waxman, S.G. Sodium channels as molecular targets in multiple sclerosis. *J. Rehabil. Res. Dev.* **2002**, *39*, 233–242. [PubMed]
94. Stafstrom, C.E. Persistent sodium current and its role in epilepsy. *Epilepsy Curr.* **2007**, *7*, 15–22. [CrossRef] [PubMed]
95. Phelan, K.; Mock, M.; Kretz, O.; Shwe, U.; Kozhemyakin, M.; Greenfield, L.; Dietrich, A.; Birnbaumer, L.; Freichel, M.; Flockerzi, V.; et al. Heteromeric canonical transient receptor potential 1 and 4 channels play a critical role in epileptiform burst firing and seizure-induced neurodegeneration. *Mol. Pharmacol.* **2011**, *81*, 384–392. [CrossRef]
96. Hubel, N.; Hosseini-Zare, M.S.; Ziburkus, J.; Ullah, G. The role of glutamate in neuronal ion homeostasis: A case study of spreading depolarization. *PLoS Comput. Biol.* **2017**, *13*, e1005804. [CrossRef]
97. Liu, Y.; Liu, S.; Zhan, F.; Zhang, X. Firing patterns of the modified Hodgkin-Huxley model subject to Taylor's formula. *Phys. A* **2020**, *547*, 124405. [CrossRef]
98. Fang, X.; Duan, S.; Wang, L. Memristive Hodgkin-Huxley spiking neuron model for reproducing neuron behaviors. *Front. Neurosci.* **2021**, *15*, 730566. [CrossRef]
99. Robertson-Anderson, R.M. Optical tweezers microrheology: From the basics to advanced techniques and applications. *ACS Macro Lett.* **2018**, *7*, 968–975. [CrossRef]
100. Lenton, I.C.D.; Scott, E.K.; Rubinsztein-Dunlop, H.; Favre-Bulle, I.A. Optical tweezers exploring neuroscience. *Front. Bioeng. Biotechnol.* **2020**, *8*, 602797. [CrossRef]
101. Kumar, R.; Valerio Vitali, V.; Wiedemann, T.; Robert Meissner, R.; Paolo Minzioni, P.; Denz, C. Multi-frequency passive and active microrheology with optical tweezers. *Sci. Rep.* **2021**, *11*, 13917. [CrossRef]
102. Kennedy, B.F. *Optical Coherence Elastography: Imaging Tissue Mechanics on the Micro-Scale*; AIP Publishing LLC: Melville, NY, USA, 2021.